NASA
Contractor Report 4383

AVSCOM
Technical Report 91-C-021

Determination of Real Machine-Tool Settings and Minimization of Real Surface Deviation by Computerized Inspection

Faydor L. Litvin, Chihping Kuan,
and Yi Zhang

GRANT NAG3-964
JULY 1991

NASA

US ARMY
AVIATION
SYSTEMS COMMAND
AVIATION R&T ACTIVITY

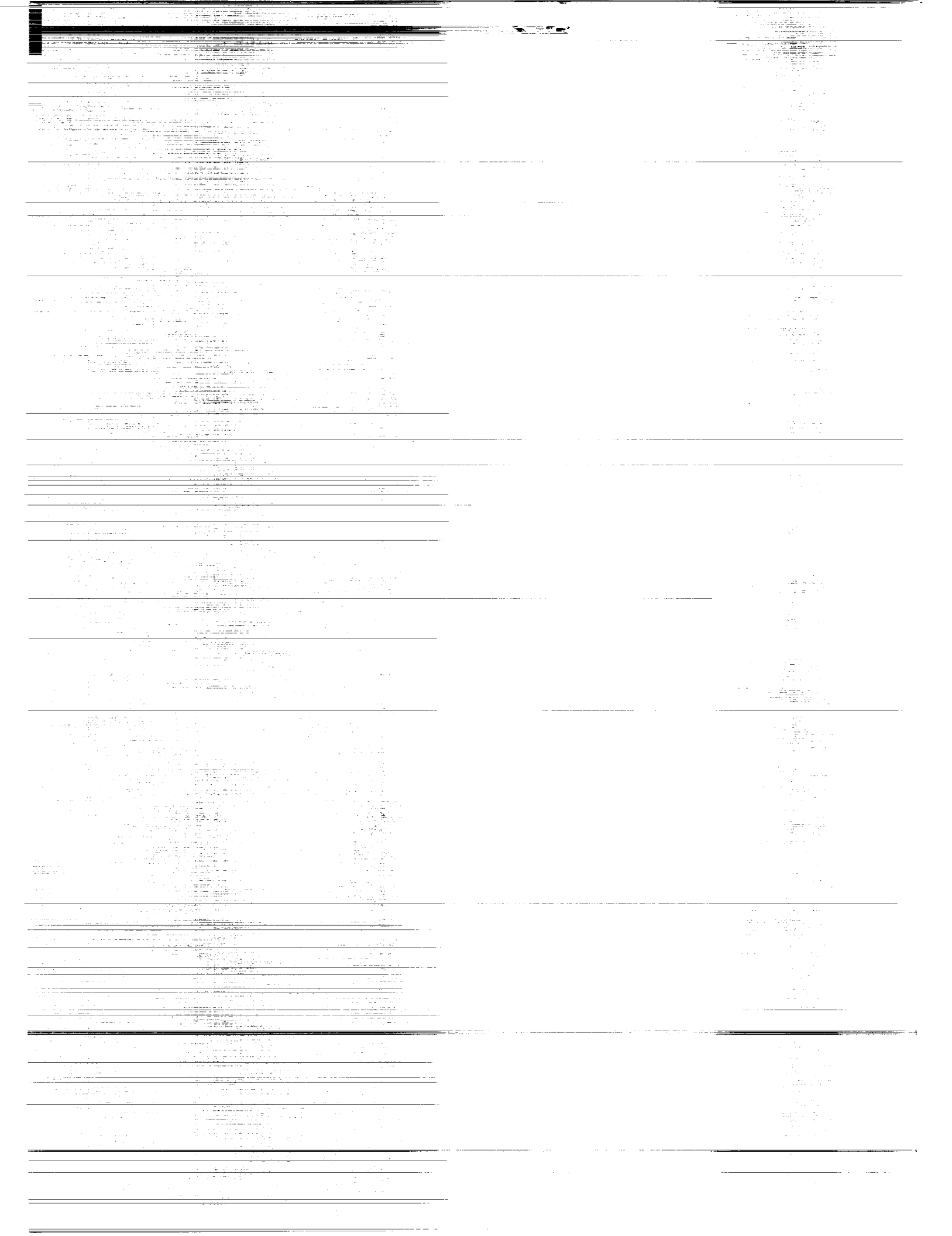

NASA
Contractor Report 4383

AVSCOM
Technical Report 91-C-021

Determination of Real Machine-Tool Settings and Minimization of Real Surface Deviation by Computerized Inspection

Faydor L. Litvin, Chihping Kuan,
and Yi Zhang
University of Illinois at Chicago
Chicago, Illinois

Prepared for
Propulsion Directorate
U.S. Army Aviation Systems Command
and
Lewis Research Center
under Grant NAG3-964

National Aeronautics and
Space Administration

Office of Management

Scientific and Technical
Information Program

1991

Table of Contents

LIST OF TABLES

LIST OF FIGURES

NOMENCLATURE

a	Radius of ball (Fig. 3.3)
A	Mean cone distance (Fig. 9.5)
ΔA	Pinion machine center to back (Fig. 9.2)
b	Normal-direction deviations of the real surface from theoretical one at the reference point, Equations (4.5-4.7)
Δb_p	Normal deviations at a measured point p (Fig. 6.1)
ΔB	Sliding base (Fig. 9.2)
b_G	Mean dedendum of pinion (Fig. 9.5)
C^2	The second order of function
CMM	Coordinate measuring machine (Fig. 3.2)
c_i	The location of the chosen cross-section, Equation (4.1)
d_j	Machine-tool settings
d_k	Machine-tool settings
E	Area of θ and u
E_m	Machine offset (Fig. 9.2)
f	Measurement data for calibration, Equation (3.1)
g	The number of surface measurements
h_m	Mean whole depth (Fig. 9.5)
H_2	Horizontal setting for gear (Fig. 8.3)
i	The tilt angle of the pinion head-cutter (Fig. 9.3)
j	The swivel angle (Fig. 9.1)
k	The number of nonlinear equations
l	Parameter of location of coordinate origin (Fig. 3.2)

$[L_{xy}]$	Free vector transformation matrix from system S_y to S_x
m	The number of parameters of applied machine-tool settings
M	Mean Point of theoretical surface Σ (Fig. 9.5)
$[M_{xy}]$	Position vector transformation matrix from system S_y to S_x
M^*	Mean point of equidistant surface $\Sigma_{(e)}$
m_{cp}	Gear cutting ratio, Equation (9.3)
n	The number of points of measurements
Δn_i	Variation of surface unit normal, Equation (9.43)
$\mathbf{n}_i$	Unit normal vector of surface Σ_i
$\mathbf{N}_i$	Normal vector of surface Σ_i
O_i	The origin of coordinate system S_i, i is the name of the system
p	The index of a measured point
q	Cradle angle (Fig. 9.1)
$\Delta \mathbf{r}_i$	Variation of surface, Equation (9.42)
$\mathbf{r}_i$	Position vector of surface Σ_i
r_G	Cutter point radius for gear (Fig. 8.1)
r_F	Cutter point radius for pinion (Fig. 9.4)
R	Radius of calibration ring (Fig. 3.3)
RL	Distance measured along the axis which is perpendicular to pinion axis (Fig. 9.5)
$\mathbf{R}$	Position vector of $\Sigma^*_{(e)}$ (Fig. 6.1)
s_F, s_G	Gaussian surfaces coordinate of pinion and gear (Fig. 9.3, 8.2)

S_i	Coordinate system with name i
S_R	Radial setting (Fig. 9.1)
V_2	Vertical setting for gear (Fig. 8.3)
u	Surface Coordinate of Σ_t (Fig. 2.2)
$\mathbf{v}^{(cp)}$	Relative sliding velocity at contact point
ΔX_m	Gear machine center to back (Fig. 8.3)
XL	Distance measured along the pinion axis (Fig. 9.5)
α_F, α_G	Cutter blade angles for pinion and gear (Fig. 9.3, 8.2)
θ_F, θ_G	Gaussian surface coordinates of pinion and gear (Fig. 9.3, 8.2)
ϕ_1	Angle of pinion rotation (Fig. 9.2)
δ	Parameter of orientation (Fig. 3.2)
Γ_1	The pinion pitch angle (Fig. 9.5)
Σ_ϕ	The family of tool surfaces
Σ_i	Theoretical surface represented in S_i (Fig. 6.1)
$\Sigma_{(c)i}$	Equidistant surface to Σ_i represented in S_i (Fig. 6.1)
Σ_i^*	Real surface represented in S_i (Fig. 6.1)
$\Sigma_{(c)i}^*$	Surface traced out by the center of probe represented in S_i (Fig. 6.1)
θ_c	Initial cradle angle, Equation (9.3)
γ_m	Machine root angle for gear (Fig. 2.3)
$\gamma_m^{(1)}$	Machine root angle for pinion (Fig. 9.2)
$\gamma_m^{(2)}$	Machine root angle for gear (Fig. 8.3)
λ	Normal distance between two surfaces, Equation (2.5)
λ_p	Normal distance between two surfaces at a measured point p (Fig. 6.1)
$\boldsymbol{\omega}^{(G)}$	Angular velocity vector of gear (Fig. 2.1)
$\boldsymbol{\omega}^{(p)}$	Angular velocity vector of pinion (Fig. 2.1)

$\boldsymbol{\omega}^{(c)}$	Angular velocity vector of cradle (Fig. 9.2)
$\boldsymbol{\rho}$	Position vector of $\Sigma_{(c)}$ (Fig. 6.1), Equation (6.1)
ρ_{ij}	The shortest distance of the chosen point of the surface from the axis of the gear, Equation (4.1)

SUMMARY

A numerical method is developed for the minimization of deviations of real tooth surfaces from the theoretical ones. The deviations are caused by errors of manufacturing, errors of installment of machine-tool settings and distortion of surfaces by heat-treatment. The deviations are determined by coordinate measurements of gear tooth surfaces. The minimization of deviations is based on the proper correction of initially applied machine-tool settings.

The contents of accomplished research project cover the following topics:

(i) Description of the principle of coordinate measurements of gear tooth surfaces.

(ii) Derivation of theoretical tooth surfaces (with examples of surfaces of hypoid gears and references for spiral bevel gears).

(iii) Determination of the reference point and the grid.

(iv) Determination of deviations of real tooth surfaces at the points of the grid.

(v) Determination of required corrections of machine-tool settings for minimization of deviations.

The procedure for minimization of deviations is based on numerical solution of an overdetermined system of n linear equations in m unknowns ($m \ll n$), where n is the number of points of measurements and m is the number of parameters of applied machine-tool settings to be corrected. The developed approach is illustrated with numerical examples.

CHAPTER 1

INTRODUCTION

The development of computer controlled machines has opened new opportunities for high precision generation of double-curvatured surfaces–gear tooth surfaces, surfaces of rotors, propellers, screws, etc. However, these opportunities can only be realized if the surface generation is complemented with coordinate measurements of the manufactured surfaces. Such measurements allow one to:

(i) Identify the real machine-tool settings and correct them if necessary (important for generation of master gears of high precision);

(ii) Determine the deviations of the real surface from the theoretical one, and minimize the deviations by correction of the initially applied machine-tool settings.

In the second case there are many factors that cause the deviations: (a) distortion of the surface by heat-treatment, (b) errors caused by deflection in the process of manufacturing, (c) errors of installment of machine-tool settings, etc. Measuring the prototype of the surface (for instance, the first gear of the being manufactured set), we can determine the deviations at n measuring points and then minimize the deviations by controlling $m \ll n$ parameters of machine-tool settings.

The Gleason Works (USA), Oerlikon (Switzerland), Caterpillar (USA), and the Ingersoll Milling Machine Company (USA), and other Companies are pioneers in the development of computer controlled machine for the generation of spiral bevel gears, hypoid gears, spur gears, helical gears,

and other objects. The Gleason Works engineers have developed an automated system and the G-AGE program for the automatic evaluation of real gear tooth surfaces that is based on measurements taken by using the Zeiss machine (Gleason Works, 1987) but without presenting the mathematical description of the procedure [1]. The Caterpillar engineers have developed their own machine for coordinate measurements and have used it for the evaluation and correction of real gear tooth surfaces (Chambers and Brown, 1987) but without presenting the algorithm and analytical method that they used in the measurement procedure for spiral bevel gears [2]. It can be expected that coordinate measurement of complicated surfaces will find wide application in industry.

The report covers the following topics:

(1) Determination of machine-tool settings for a real surface. Here it is assumed that the deviations of the real surface form the theoretical one are caused only by the errors of machine-tool settings. The proposed approach allows the required corrections of machine-tool setting to be determined based on the data of coordinate measurements. The solution to this problem is significant for generation of master-gears of high precision.

(2) Determination of corrections of machine-tool settings for a real surface with irregular deviations. Such deviations can be caused by heat-treatment, deflection in the course of manufacturing, and other factors. The proposed approach assumes that the manufacturing process provides repeatable surface deviations due to stable conditions of gear manufacturing and heat treatment and allow the deviations to be minimized by appropriate corrections to the machine-tool settings.

The proposed approaches cover the solutions to the above-mentioned problems and are illustrated by numerical examples for hypoid pinion and gear tooth surfaces.

The contents of the report is divided into two parts:

I. *General Theory*

In part I, the successful application of coordinate measurements needs the following procedures :

(i) Analytical or numerical representation in the 3D space of the theoretical surface and the equidistant surface where the center of the probe is located in the process of measurements.

(ii) Determination of the grid where the center of the probe must be located.

(iii) A certain point on the theoretical surface must be chosen as the reference point.

(iv) Determination of deviations of the real tooth surface from the theoretical one that are measured along the common normal to both surfaces.

(v) Minimization of deviations of the real surface by correction of previously applied machine-tool settings.

II. *Application to Coordinate Measurements of Hypoid Pinions and Gears.*

Part I

GENERAL THEORY

CHAPTER 2

REPRESENTATION OF A THEORETICAL SURFACES

Henceforth, we will consider four surfaces: (i) Σ–the theoretical tooth surface, (ii) $\Sigma_{(e)}$–the surface that is equidistant to Σ and might be traced out by the probe center if the deviations are equal to zero, (iii) $\Sigma^{\star}$–the real tooth surface, and (iv) $\Sigma^{\star}_{(e)}$–the surface that is traced out by the probe center when the real surface is measured. The subscript for symbols $\Sigma, \Sigma_{(e)}, \Sigma^{\star}$ and $\Sigma^{\star}_{(e)}$ (for instance $\Sigma_{(e)m}$) indicates in which coordinate system (S_m for designation $\Sigma_{(e)m}$) the surface is represented.

We consider that a theoretical surface Σ_t is represented analytically in a coordinate system S_t that is rigidly connected to Σ_t. Two types of representation arise:

(i) in two-parametric form by a vector function

$$\mathbf{r}_t(u, \theta) \tag{2.1}$$

and (ii) in three-parametric form with related parameters.

$$\mathbf{r}_t(u, \theta, \phi) \tag{2.2}$$

$$f(u, \theta, \phi) = 0 \tag{2.3}$$

Equations (2.2) and (2.3) represent Σ_t as the envelope to the family of tool surfaces, Σ_ϕ, that is generated in coordinate system S_t by the tool surface in its relative motion with respect to the being-generated gear. Parameters (u, θ) in expressions (2.2) and (2.3) are the Gaussian coordinates (surface coordinates) of the tool; ϕ is the generalized parameter of motion. Equation (2.3) is the equation of meshing (Litvin, 1989) [3]. In the case where the tool surface is a ruled developable surface, for example a cylindrical involute surface, a screw involute surface, or a cone, the equation of meshing is linear in one of the surface parameters and it is easy to represent the generated surface directly in a two-parametric form.

Henceforth, we will consider that the theoretical surface is represented in two-parametric form as follows.

$$\mathbf{r}_t(u, \theta; d_j) \epsilon C^2 \quad (j = 1, \ldots, m); \quad u, \theta \epsilon E; \quad \frac{\partial \mathbf{r}_t}{\partial u} \times \frac{\partial \mathbf{r}_t}{\partial \theta} \neq 0 \tag{2.4}$$

The designation C^2 means that the vector function has continuous derivatives for all arguments at least to the second order. The Gaussian coordinates are designated by u and θ, and E is the area of u and θ. The inequality in (2.4) indicates that Σ_t is a regular surface. The designation d_j $(j = 1, \ldots, m)$ indicates constant parameters–the so-called machine-tool settings.

To illustrate d_j we consider the case of generation of a formate cut hypoid gear (Fig. 2.1). The generating surface is a cone with Gaussian coordinates u and θ (Fig. 2.2). The installation of the cone with respect to the cradle is determined with two parameters, H_2 and V_2 (Fig. 2.3). The installation of the gear in the plane $y_c = 0$ is determined with the parameters $\triangle X_m$ and γ_m. Here: $\triangle X_m$ represents the location of the crossing point, O_t, with respect to the machine center, O_c;

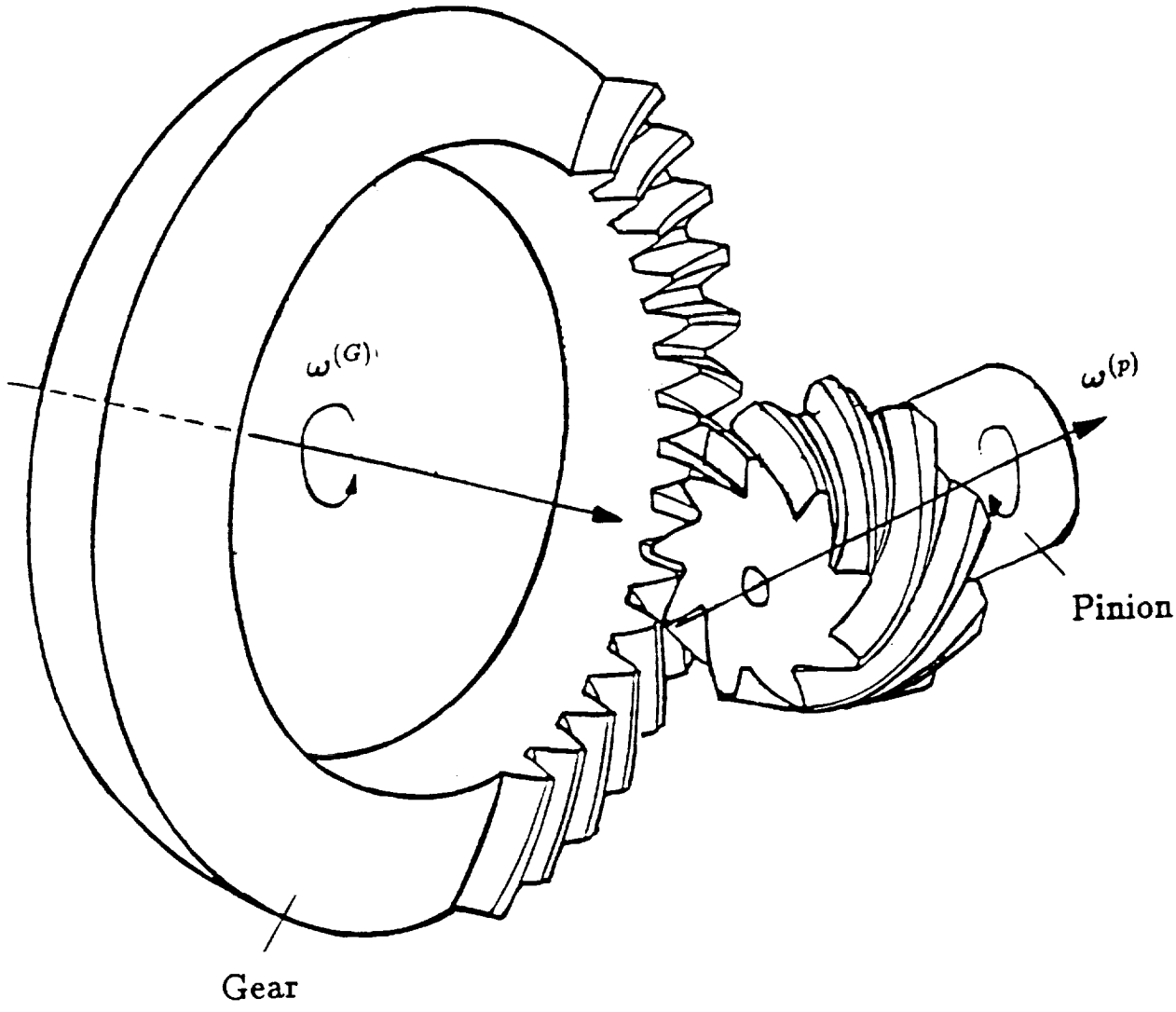

Figure 2.1: Hypoid Gear Drives

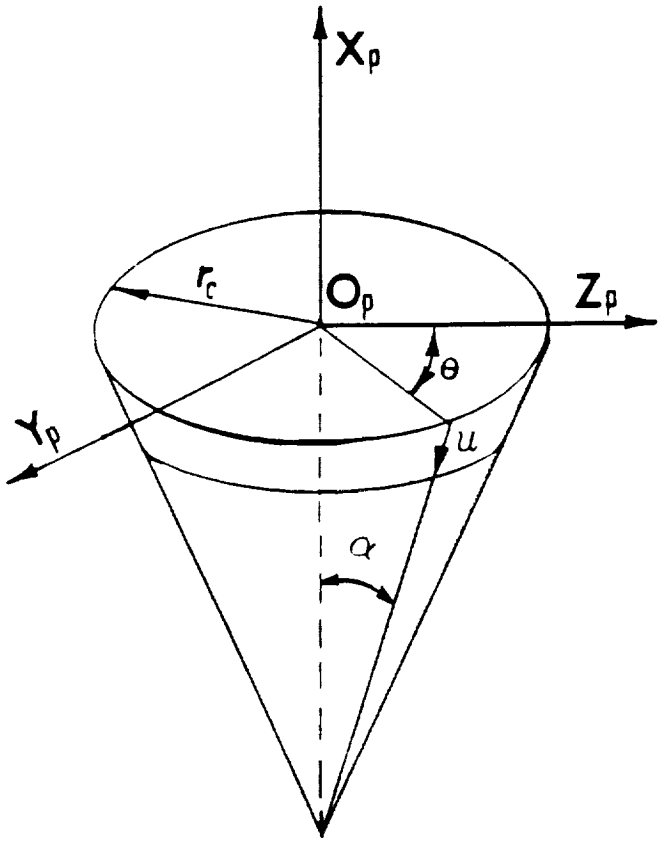

Figure 2.2: Generating Cones

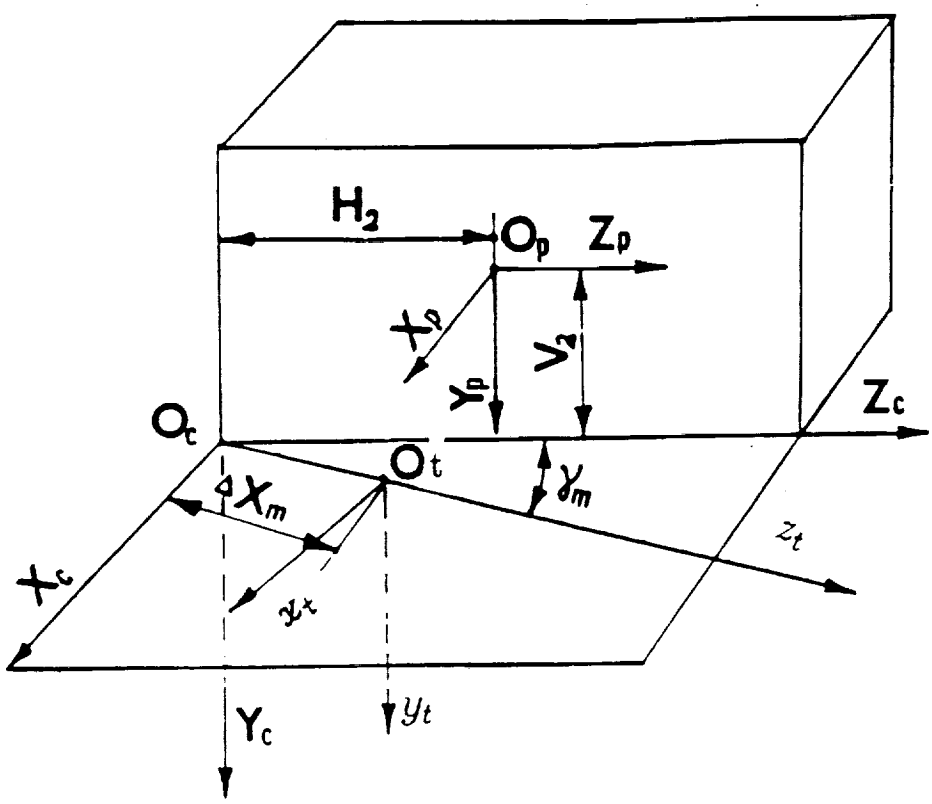

Figure 2.3: Machine-Tool Settings For Formate Cut Gear

and γ_m determines the orientation of gear axis z_t in the process of generation. These parameters, $H_2, V_2, \triangle X_m$ and γ_m, are the machine-tool settings, d_j. It is assumed that the parameters d_j can be varied to minimize the deviations of the real tooth surface to the theoretical one.

In addition to expression (2.4) we will also need a parametric representation of a surface $\Sigma_{(e)t}$ that is equidistant to the theoretical surface Σ_t. Such a surface is represented by:

$$\mathbf{r}_t(u,\theta) + \lambda \mathbf{n}_t(u,\theta) \quad (\lambda \neq 0) \tag{2.5}$$

Here:

$$\mathbf{n}_t(u,\theta) = \frac{\mathbf{N}_t}{|\mathbf{N}_t|}; \qquad \mathbf{N}_t = \frac{\partial \mathbf{r}_t}{\partial u} \times \frac{\partial \mathbf{r}_t}{\partial \theta} \neq 0 \tag{2.6}$$

where $\mathbf{N}_t$ is the vector of surface normal; $\mathbf{n}_t$ is the unit normal; and λ is a scalar that determine the distance between the two surfaces that is measured along the normal.

Examples of derivation of surfaces of spiral bevel gears have been represented in the works: F.L. Litvin [3] F.L. Litvin and Y. Zhang [4], and R.F Handschuh and F.L. Litvin [5].

CHAPTER 3

PRINCIPLE OF COORDINATE MEASUREMENT

The machine for coordinate measurements (CMM) usually has four or more degrees of freedom. For instance, the Zeiss machine used by the Gleason Works has four degrees of freedom, one rotational and three translational motions [1]. The three computer controlled translational motions of the probe are performed in three mutually-perpendicular directions during the process of measurements. The probe tip is a changeable ball whose diameter can be chosen from a wide range, according to the specifications of the surfaces to be measured. In the Zeiss machine, the rotational motion is performed by a rotary table whose axis coincides with the axis of the workpiece and can be rotated together with the workpiece being measured.

Henceforth, we will consider that a coordinate system $S_m(x_m,y_m,z_m)$ is rigidly connected to the computer controlled 3-dimensional coordinate measuring machine (CMM) and z_m coincides with the axis of the gear and pinion (Fig. 3.1). The axis of the probe may be installed parallel to z_m (Fig. 3.1.a) or perpendicular to z_m (Fig. 3.1.b), depending on the design of the workpiece and the surface (for instance, depending on the pitch cone angle of the gear or the pinion). The back face of the workpiece, which is perpendicular to its axis and is finished to high precision, is installed flush with the base plane of the CMM. The origin of the coordinate system S_m can be located in the base plane or is related with it.

A Coordinate system $S_t(x_t, y_t, z_t)$ is rigidly connected to the being measured gear. In some

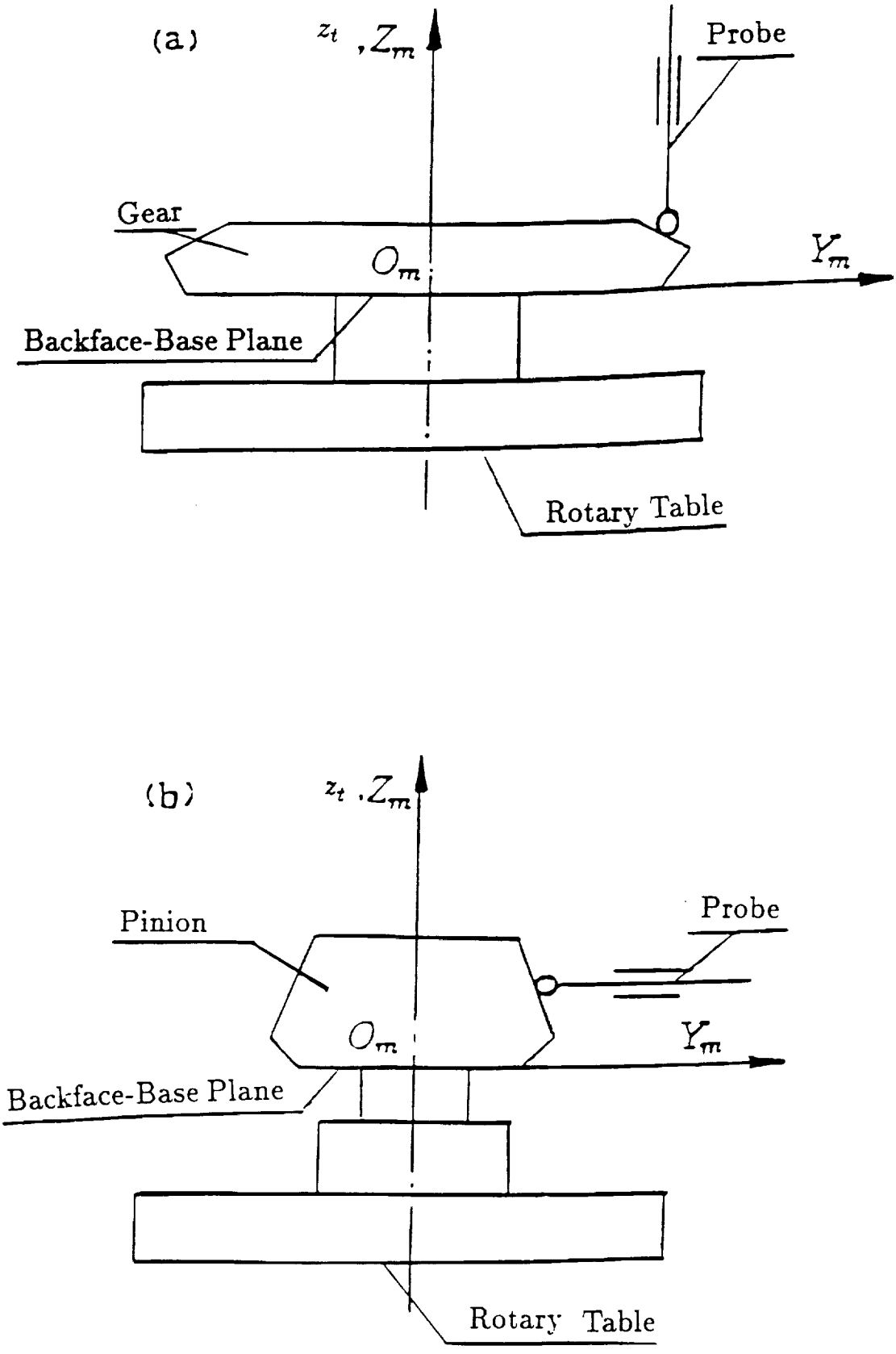

Figure 3.1: Surface Measurement of a Gear and Pinion

cases we may assume that the origin O_t coincide with O_m. Thus, the two coordinate systems S_m and S_t can be brought into alignment only by the rotation of the rotary table. In the most general case, the orientation and location of S_t respect to S_m are determined with two parameters δ and l (Fig. 3.2). We will consider that parameter l is known from the installments and parameter δ is determined by using the procedure of computation described below (in chapter 4).

In order to align the coordinate system of tooth surface S_t with the CMM coordinate system S_m, a reference point, say $(x_m^{(0)}, y_m^{(0)}, z_m^{(0)})$ on the theoretical tooth surface, say Σ_m , must be specified. The coordinates $(X_m^{(0)}, Y_m^{(0)}, Z_m^{(0)})$ of the probe center, which correspond to $(x_m^{(0)}, y_m^{(0)}, z_m^{(0)})$ can be determined knowing the radius of the probe and the normal to the surface by using equation (2.5). For the initial installment of the tooth surface, the probe center is placed at $(X_m^{(0)}, Y_m^{(0)}, Z_m^{(0)})$, and the tooth surface is brought into contact with the probe by turning the rotary table. Therefore, the tooth surface is fixed in the process of measurements and the probe performs measurements by translational motion. The displacement of the probe center in the x_m, y_m and z_m axis directions represent its displacements from the initial position.

The measurement data provide the coordinates, $(X^\star, Y^\star, Z^\star)$ of the probe center, which traces out in reality an equidistant surface, say $\Sigma_{(c)}^\star$, to the real tooth surface, say $\Sigma^\star$, in the process of measurement.

Knowing the initial and current positions of the probe center, we can determine the surface deviations based on the change of position of the center of the probe in the process of measurements.

CMM Calibration:

Calibration of the CMM for a chosen probe ball can be accomplished using a calibration ring (Fig. 3.3). The initial coordinates of the center of the ball are:

$$[X_m^{(0)}, Y_m^{(0)}, Z_m^{(0)}] = [R + a, 0, f] \tag{3.1}$$

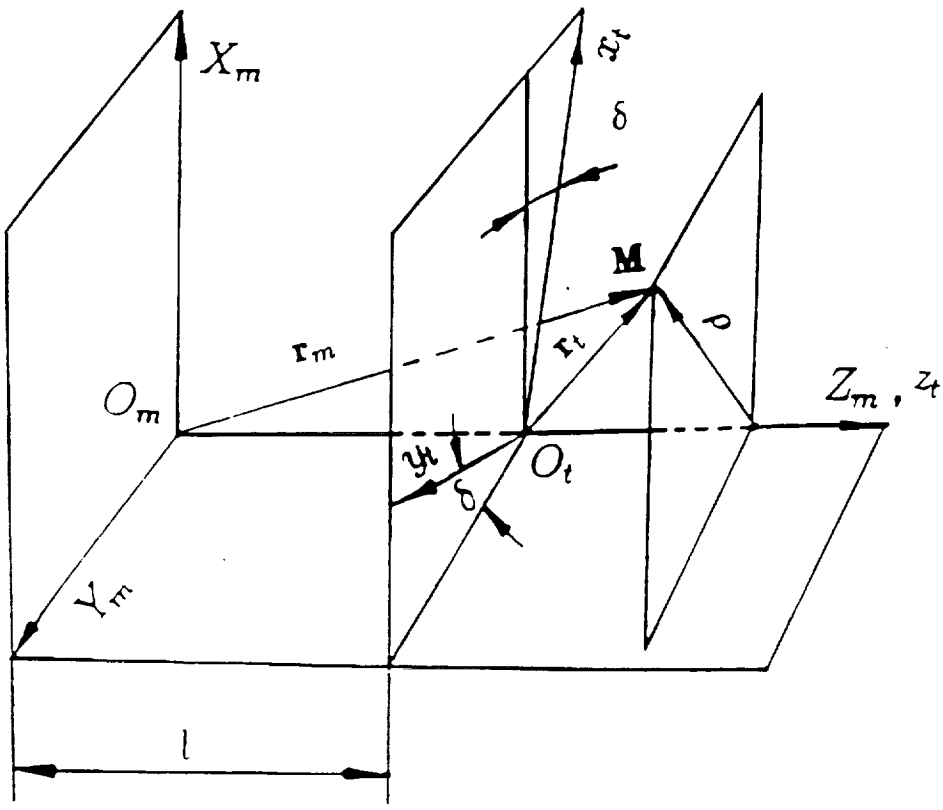

Figure 3.2: Orientation of CMM Coordinate System S_m and Workpiece Fixed Coordinate System S_t

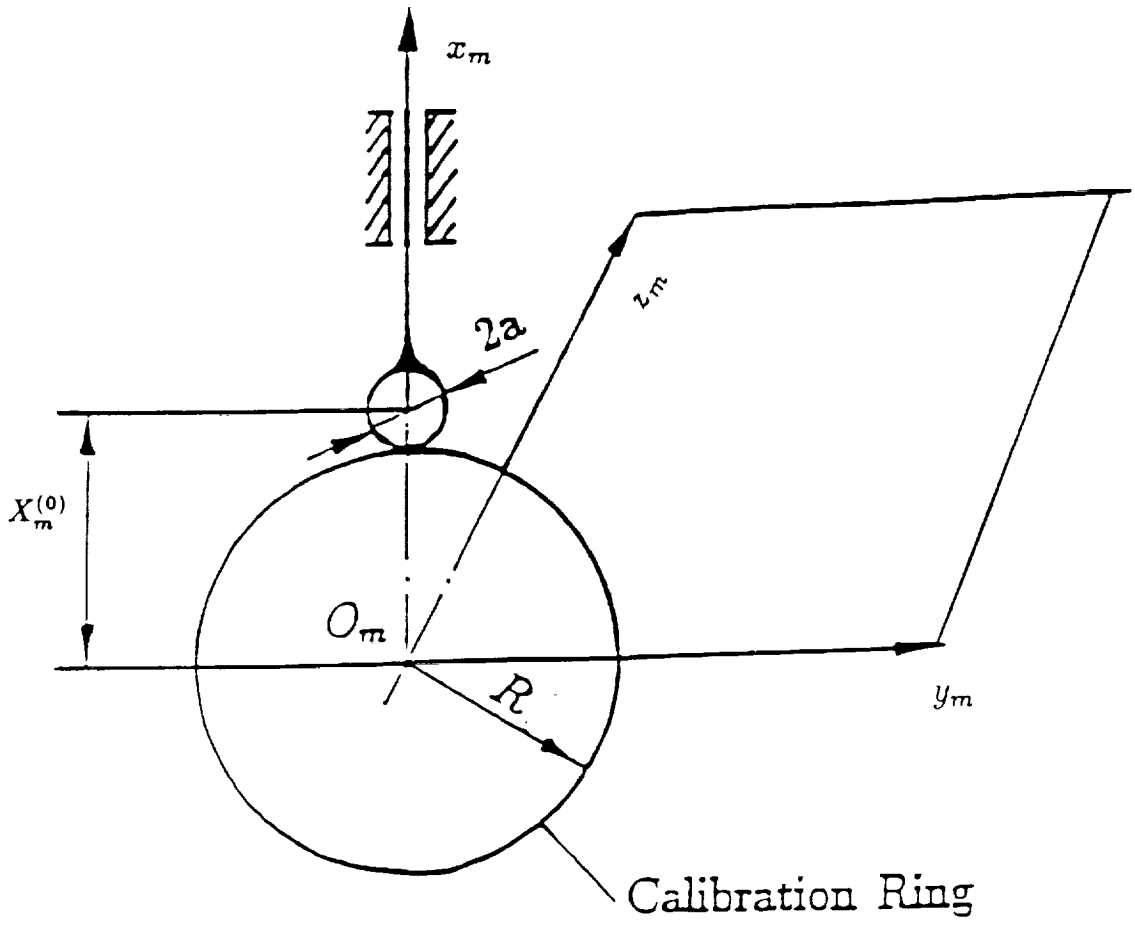

Figure 3.3: Calibration of CMM for Measurements Using a Calibration Ring

Here R is the radius of the calibration ring and a is the radius of the ball. At the initial position, the probe ball is in contact with the calibration ring. The $y_m = 0$ alignment can be achieved if the same displacement $\triangle x_m$ of the probe corresponds to $\pm\triangle y_m$ displacements. The value of f can be obtained by independent measurement.

CHAPTER 4

THE GRID AND REFERENCE POINT

4.1 The Grid

The grid (Fig. 4.1) is a set of points on the theoretical surface Σ_t that are chosen as points of contact between the tooth surface and the probe [6]. Figure 4.2 shows the grid on the surface of a spiral bevel gear.

(1). In accordance to the practice of measurements a set of 45 points is usually chosen for the measurements that are located in nine longitudinal cross-sections of the gear and pinion surface with five points in each cross-section (Fig. 4.2).

(2). Consider that the theoretical surface Σ_t is represented in two-parametric form by the vector function $\mathbf{r}_t(u,\theta)$. Then the Gaussian coordinates for the grid points can be determined based on the following considerations.

$$\left.\begin{aligned} z_t(u,\theta) &= c_i \\ x_t^2(u,\theta) + y_t^2(u,\theta) &= \rho_{ij}^2 \end{aligned}\right\} \tag{4.1}$$

Here: c_i is the constant that determines the location of the chosen cross-section; ρ_{ij} determines the shortest distance of the chosen point of the surface from the axis of the gear.

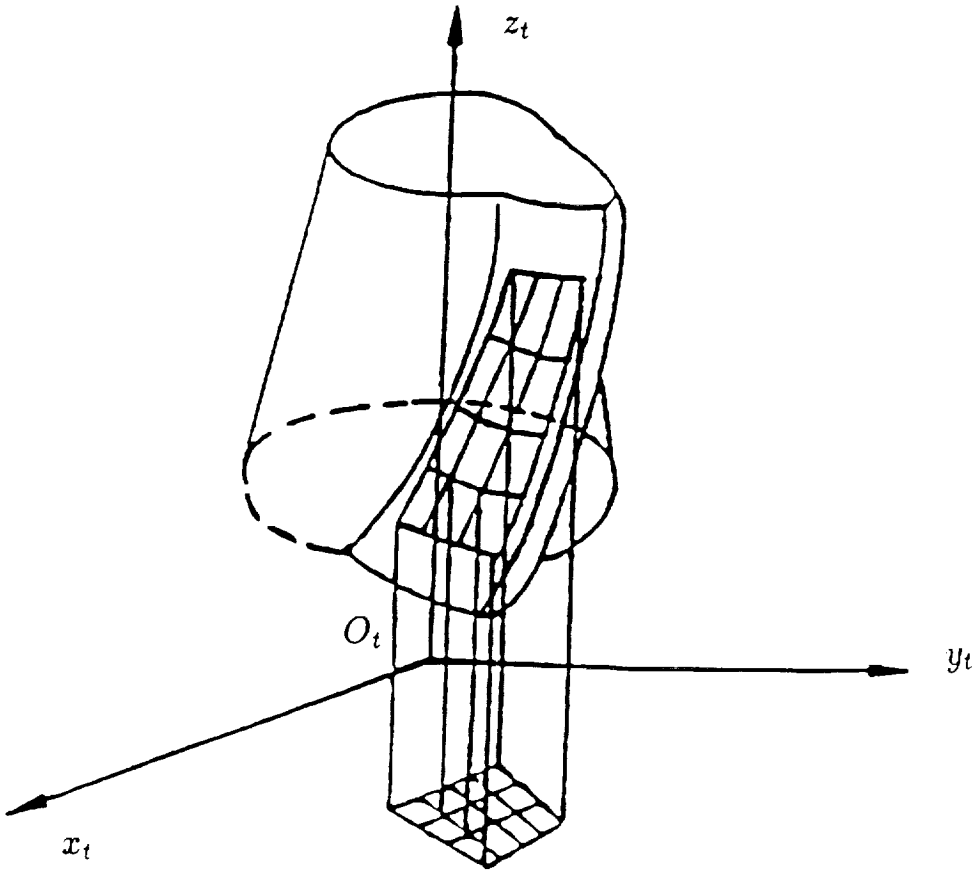

Figure 4.1: Grid on Theoretical Surface Σ_t

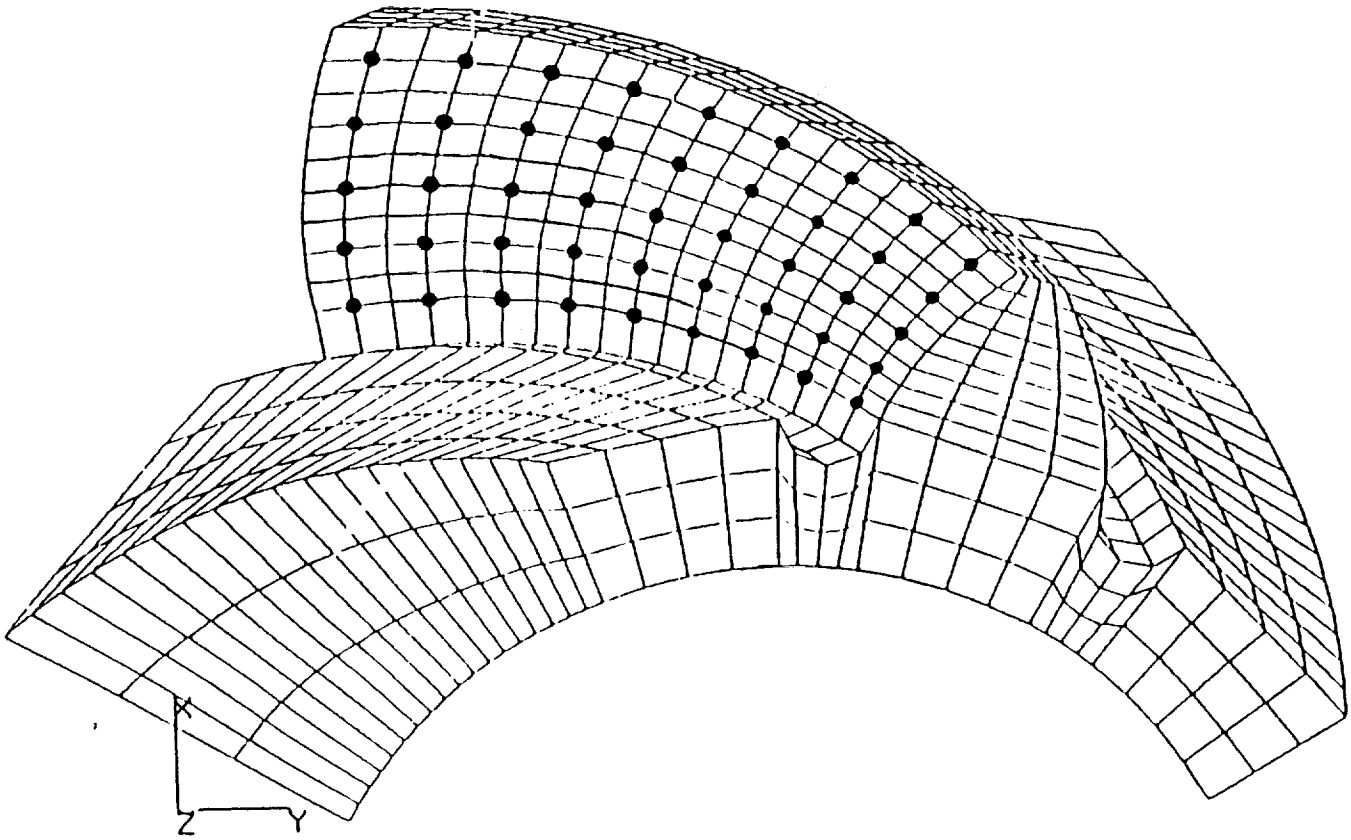

Figure 4.2: Surface Grid on a Spiral Bevel Gear

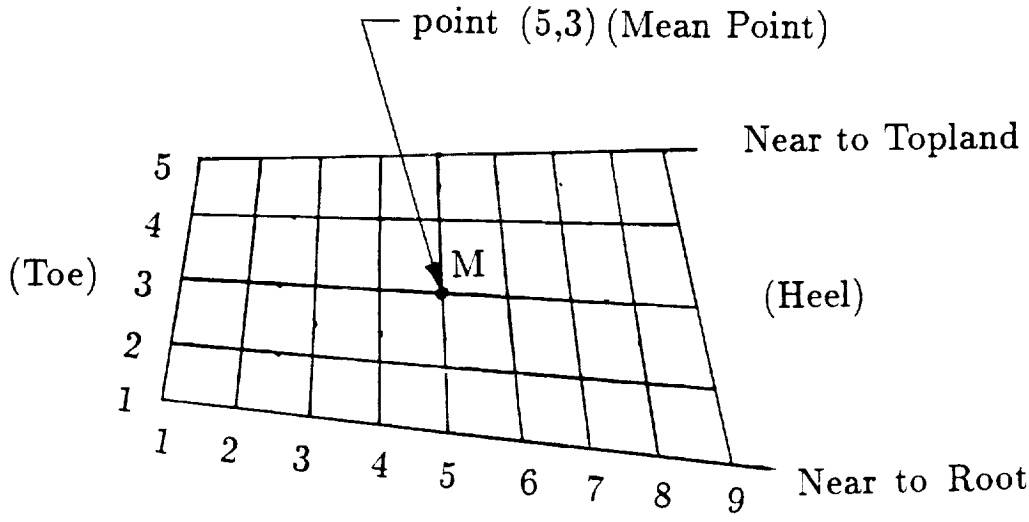

Figure 4.3: Definition of Points on the Measurement Grids

We can determine the Cartesian coordinates and curvilinear coordinates (u, θ) for $n = i \times j$ points of measurements.

(3). The theoretical coordinates of the probe center for each grid point is determined by considering that the probe center will lie on a surface Σ_e that is equidistant from Σ_t. The following vector equation determines these coordinates in system S_t.

$$\boldsymbol{\rho}_t = \mathbf{r}_t(u, \theta) + a\mathbf{n}_t(u, \theta) \tag{4.2}$$

where a is the radius of the ball surface of the probe. Equations (4.2) represent in S_t the surface that might be traced out by the center of the probe if the surface deviations are equal to zero.

4.2 Reference Point

One of the grid points (usually the center one, i.e., mean point) is chosen as the reference point (Fig. 4.3). This point is used to install the gear on the CMM and to obtain the value of δ that is needed to represent the coordinates of the grid points in S_m. The CMM is provided with a rotary table that allows the gear to be rotated to an initial position with respect to the probe.

We consider that the gear is installed with its back-face flush against the base plane of the CMM such that the O_m coincides with the O_t and the parameter $l = 0$ is known (Fig. 3.2). The rotational alignment of the gear and the value of δ can be obtained based on following two steps.

Step (i): the probe is brought into contact with the point on the real surface that is closest to the chosen reference point.

Step (ii): the parameter δ is determined based on coordinate measurements at this point.

We assume that the real surface deviations from the theoretical one and that we would like the

probe to contact with the real surface at the point closest to the chosen *reference* point. Assuming that the variation in surface normal will be small, the measured coordinates $(X_m^{(0)}, Y_m^{(0)}, Z_m^{(0)})$ of the probe center can represented by using the following matrix equation (Fig. 3.2).

$$\mathbf{R}_m^{(0)} = [M_{mt}]\boldsymbol{\rho}_t^{(0)} \tag{4.3}$$

$$[M_{mt}] = \begin{bmatrix} \cos\delta & \sin\delta & 0 & 0 \\ -\sin\delta & \cos\delta & 0 & 0 \\ 0 & 0 & 1 & 0 \\ 0 & 0 & 0 & 1 \end{bmatrix} \tag{4.4}$$

Then we obtain

$$X_m^{(0)} = (X_t^{(0)} + bn_{xt})\cos\delta + (Y_t^{(0)} + bn_{yt})\sin\delta \tag{4.5}$$

$$Y_m^{(0)} = -(X_t^{(0)} + bn_{xt})\sin\delta + (Y_t^{(0)} + bn_{yt})\cos\delta \tag{4.6}$$

$$Z_m^{(0)} = Z_t^{(0)} + bn_{zt} \tag{4.7}$$

Here: $(\boldsymbol{\rho}_t^{(0)}=[X_t^{(0)}, Y_t^{(0)}, Z_t^{(0)}]^T)$ are coordinates of the point equidistant from the chosen reference point as given by (4.2); (n_{xt}, n_{yt}, n_{zt}) are the components of the theoretical surface normal in S_t at the chosen reference point; δ is the parameter of orientation; and b is the normal-direction deviation of the real surface from the theoretical surface at the chosen reference point.

Together, equations (4.5–4.7) represent a system of 3 equations in 5 unknowns, $X_m^{(0)}, Y_m^{(0)}, Z_m^{(0)}, \delta$ and b, that can not be solved uniquely. To obtain a solution we assume that at reference point $b = 0$, and for convenience we choose $Y_m^{(0)} = 0$. Then equation (4.7) can be solved for $Z_m^{(0)} = Z_t^{(0)}$ and from equations (4.5) and (4.6) we can derive the following relation for $X_m^{(0)}$ that does not depend on δ.

$$X_m^{(0)} = \sqrt{(X_t^{(0)})^2 + (Y_t^{(0)})^2} \tag{4.8}$$

After solving (4.8) for $X_m^{(0)}, \delta$ can be determined from the following relation that can be derived from equations (4.5) and (4.6) considering that $Y_m^{(0)} = b = 0$.

$$\tan\frac{\delta}{2} = -\frac{(X_t^{(0)})^2 + (Y_t^{(0)})^2 - Z_t^{(0)} X_m^{(0)}}{Y_t^{(0)} X_m^{(0)}} \tag{4.9}$$

Based on the above considerations, rotational alignment of the gear can be obtained as follows:

(i) install the probe with coordinates $(X_m^{(0)}, Y_m^{(0)}, Z_m^{(0)})$ that have been determined as described above;

(ii) turn the rotary table until the probe contact the to-be measured surface. The value of δ for this installation is given by equation (4.9).

Process of Measurements

With the parameters δ and l determined, matrix equation that is similar to (4.3) can be used to find the S_m-system coordinates , X_m, Y_m, Z_m, of the theoretical probe center for each grid point.

In the process of measurement, the probe center is controlled by the CMM to keep two measured coordinates, say $(X_m^\star, Y_m^\star)$ as close to the coordinates (X_m, Y_m) of the chosen grid point as possible. The third measured coordinate $Z_m^\star$ will differ from Z_m if the real tooth surface deviates from theoretical one.

CHAPTER 5

DETERMINATION OF REAL MACHINE-TOOL SETTINGS

5.1 Initial Considerations

The determination of real machine-tool settings is for the case when surface deviations are caused only by errors in the installment of machine-tool settings. It is especially important for the generation of a master gear–a gear that is used as a model for the evaluation of manufactured gears. In this section we use the deviations determined by coordinate measurements to determine the real machine-tool settings and then to correct the installment of machine-tool settings.

In addition to the real machine-tool settings, we consider the parameters δ and l (Fig. 3.2) as unknowns.

The imaginary surface $\Sigma_{(a)}$ that is equidistant to the theoretical surface Σ is represented in S_t by (see equations 4.2):

$$\left.\begin{aligned} X_t &= x_t(u,\theta;d_j) + an_{xt}(u,\theta;d_j) = A(u,\theta;d_j) \\ Y_t &= y_t(u,\theta;d_j) + an_{yt}(u,\theta;d_j) = B(u,\theta;d_j) \\ Z_t &= z_t(u,\theta;d_j) + an_{zt}(u,\theta;d_j) = C(u,\theta;d_j) \end{aligned}\right\} \tag{5.1}$$

Here: a is the radius of the probe sphere; A, B and C represent the resulting functions; and d_j $(j = 1, \ldots, m)$ are the to-be-determined real machine-tool settings that have been applied in the process of generation.

Basic Equations

The determination of the real machine-tool settings is based on the following procedure.

Step 1. The coordinate transformation from S_t to S_m which is rigidly connected to the coordinate measuring machine is based on the matrix equation:

$$\mathbf{r}_{(e)m} = [M_{mt}]\mathbf{r}_{(e)t} \tag{5.2}$$

where $[M_{mt}]$ is represented by equation (4.4).

Considering that the measured coordinates of the probe center $(X_m^\star, Y_m^\star, Z_m^\star)$ coincide with coordinates (X_m, Y_m, Z_m) on the theoretical equidistant surface $\Sigma_{(e)m}$ represented in S_m we have

$$[X_m \quad Y_m \quad Z_m]^T = [X_m^\star \quad Y_m^\star \quad Z_m^\star]^T \tag{5.3}$$

Equations (5.1), (5.2) and (5.3) yield

$$\left.\begin{aligned} X_m^\star &= A(u,\theta;d_j)\cos\delta + B(u,\theta;d_j)\sin\delta \\ Y_m^\star &= -A(u,\theta;d_j)\sin\delta + B(u,\theta;d_j)\cos\delta \\ Z_m^\star &= C(u,\theta;d_j) + l \end{aligned}\right\} \tag{5.4}$$

Step 2. Our goal is to derive equations that are invariant with respect to the parameters δ and l. Equation (5.4) yield

$$X_m^{\star 2} + Y_m^{\star 2} = A^2(u,\theta;d_j) + B^2(u,\theta;d_j) \tag{5.5}$$

$$\tan\frac{\delta}{2} = \frac{A(A - X_m^\star) + B(B - Y_m^\star)}{BX_m^\star - AY_m^\star} \tag{5.6}$$

It is also evident that

$$l = Z_m^\star - C(u,\theta;d_j) \tag{5.7}$$

Step 3. Henceforth we will drop the subscript m indicating that the coordinates of a point are represented in coordinate system S_m. We will designate with g the number of measurement points and with subscript p the index of a measured point. Based on equations (5.5), (5.6) and (5.7), we obtain the following system of equations that is used for determination of the real machine-tool

settings.

$$X_p^{\star 2} + Y_p^{\star 2} = A^2(u_p, \theta_p; d_j) + B^2(u_p, \theta_p; d_j) \qquad (p = 1, \ldots, g) \tag{5.8}$$

$$\frac{A_p(A_p - X_p^\star) + B_p(B_p - Y_p^\star)}{B_p X_p^\star - A_p Y_p^\star} = \frac{A_{p+1}(A_{p+1} - X_{p+1}^\star) + B_{p+1}(B_{p+1} - Y_{p+1}^\star)}{B_{p+1} X_{p+1}^\star - A_{P+1} Y_{p+1}^\star} \tag{5.9}$$

$(1 \leq p \leq g - 1)$

$$Z_{p+1}^\star - Z_p^\star = C(u_{p+1}, \theta_{p+1}; d_j) - C(u_p, \theta_p; d_j) \qquad (1 \leq p \leq g - 1) \tag{5.10}$$

Using the results of measurements for g points on the surface we obtain $(3g - 2)$ equations (5.8), (5.9) and (5.10) in: (i) $2g$ unknown surface coordinates (u_p, θ_p); and (ii) m unknown machine-tool settings d_j $(j = 1, \ldots, m)$. Thus, to determine m unknown machine-tool settings we need:

$$g = m + 2; \qquad k = 3g - 2 = 3m + 4 \tag{5.11}$$

where g is the number of surface measurements and k is the number of nonlinear equations that have to be solved. Parameters δ and l of orientation and location of coordinate system S_t with respect to S_m (Fig. 3.2). can be determined from equations (5.6) and (5.7).

In the case when the gear and the pinion are installed flush against the base plane of the CMM we can take $l = 0$ (the origin O_t coincides with O_m), and use the equation:

$$Z_p^\star = C(u_p, \theta_p; d_j) \tag{5.12}$$

in place of equation (5.10). For this case, the coordinate measurements of g points on the real surface, results in $(3g - 1)$ equation (5.8), (5.9) and (5.12), in $2g$ unknown surface coordinates (u_p, θ_p), and m unknown machine-tool settings d_j $(j = 1, \ldots, m)$. To determine the m unknown machine-tool settings we need

$$g = m + 1 \qquad k = 3g - 1 = 3m + 2 \tag{5.13}$$

5.2 Computational Procedure

The numerical solution of a large system of nonlinear equations is a complicated problem. For the case where $l \neq 0$ and $m = 4$, the number of equations to be solved is $k = 16$. The system of nonlinear equations can be solved using computer software such as the IMSL subroutine DNEQNF [7]. However, the successful application of this program requires a good first guess– an initial set of unknowns that is used for the first iteration. We propose a solution procedure that begins with a system of four equations using the measurements for only two points on the surface. The number of equations, $k = 4$, and the number of measurements, $g = 2$, can be obtained from equation (5.11) considering that $m = 0$. This means that for the first step, errors in the machine-tool settings are neglected – the machine-tool variables $d_1, d_2, \ldots, d_m$ in equation (5.8), (5.9) and (5.10) are set to

the nominal values $d_1^{(0)}, d_2^{(0)}, \ldots, d_m^{(0)}$.

Step 1. An initial guess for the system of 4 equations is obtained as follows: (i) an approximate value for l is determined by measurements, then (ii) neglecting the errors of machine-tool settings, approximate values for the surface coordinates of two measured points are determined using the following equations.

$$C(u_p, \theta_p) = Z_p^\star - l \qquad (p = 1, 2) \tag{5.14}$$

$$A^2(u_p, \theta_p) + B^2(u_p, \theta_p) = X_p^{\star 2} + Y_p^{\star 2} \qquad (p = 1, 2) \tag{5.15}$$

Step 2. Knowing the approximate values of (u, θ) for the two points of measurement, we then obtain more precise solutions for surface coordinates using th system of four equations:

$$A^2(u_1, \theta_1) + B^2(u_1, \theta_1) = X_1^{\star 2} + Y_1^{\star 2} \tag{5.16}$$

$$A^2(u_2, \theta_2) + B^2(u_2, \theta_2) = X_2^{\star 2} + Y_2^{\star 2} \tag{5.17}$$

$$C_2(u_2, \theta_2) - C_1(u_1, \theta_1) = Z_2^\star - Z_1^\star \tag{5.18}$$

$$\frac{A_1(A_1 - X_1^\star) + B_1(B_1 - Y_1^\star)}{B_1 X_1^\star - A_1 Y_1^\star} = \frac{A_2(A_2 - X_2^\star) + B_2(B_2 - Y_2^\star)}{B_2 X_2^\star - A_2 Y_2^\star} \tag{5.19}$$

obtained from equation (5.8), (5.9) and (5.10) considering that $g = 2$, and neglecting errors in the machine-tool settings.

Step 3. The solution obtained for the previous step is then used as the initial guess for a larger system of $k = 7$ equations (5.8), (5.9) and (5.10), obtained by considering that one machine-tool setting is a variable, and using $g = 3$ measurement points.

Step 4. Gradually the number of machine-tool settings that are considered as variables are increased until eventually the exact values for the whole set of $j = 1, \ldots, m$ unknowns machine-tool settings are determined using a system of $k = 3m + 4$ equations (5.8), (5.9) and (5.10). Knowing the real values of the machine-tool settings we may correct the settings and eliminate the deviations of the real surface from the theoretical one.

We can expect that in some cases the real tooth surface will be substantially distorted due to errors other than errors in the applied machine-tool settings. For these cases, we use the procedure described in chapter 6 and 7 to improve the precision of the generated surface.

CHAPTER 6

DETERMINATION OF DEVIATIONS OF REAL TOOTH SURFACE

Let us consider in coordinate system S_m two surfaces: (i) $\Sigma_{(e)m}$ that might be traced out in S_m by the center of the probe if the gear tooth surface is an ideal surface, and (ii) surface $\Sigma^{\star}_{(e)m}$ that is traced out by the center of the probe in the case when the gear tooth surface is the real surfaces (Fig. 6.1).

The position vector of the probe center for the theoretical equidistant surface $\Sigma_{(e)m}$ is determined in S_m with the equation similar to (4.2), i.e.,

$$\boldsymbol{\rho}_{mp} = \mathbf{r}_{mp}(u_p, \theta_p, d_j^{(0)}) + a\mathbf{n}_{mp}(u_p, \theta_p, d_j^{(0)}) \qquad (p = 1, \ldots, 45 \;\; ; \;\; j = 1, \ldots, m) \tag{6.1}$$

where, subscript p is the index of a measured point.

By measurements of the real surface the position vector of the probe center may be represented as

$$\mathbf{R}^{\star}_{mp} = \mathbf{r}_{mp}(u_p, \theta_p, d_j^{(0)}) + \lambda_p \mathbf{n}_{mp}(u_p, \theta_p, d_j^{(0)}) \qquad (p = 1, \ldots, 45 \;\; ; \;\; j = 1, \ldots, m) \tag{6.2}$$

where λ_p determines the real location of the probe center on surface $\Sigma^{\star}_{(e)m}$ and is considered along the normal to the theoretical surface Σ_m.

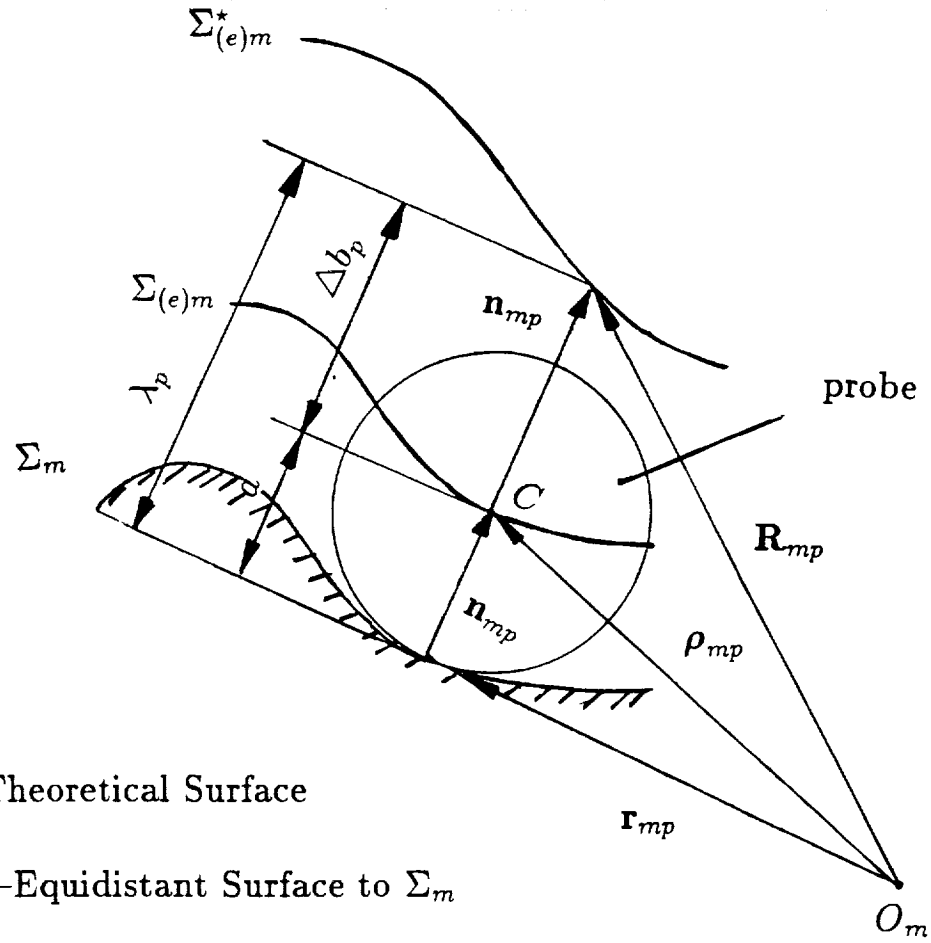

Σ_m–Theoretical Surface

$\Sigma_{(e)m}$–Equidistant Surface to Σ_m

$\Sigma^{\star}_{(e)m}$–Surface Traced Out By the Center of Probe

Figure 6.1: Surface Notations

Subscript "m" indicates that both surfaces are represented in S_m; $\mathbf{r}_{mp}$ is the position vector of the theoretical tooth surface Σ_m; subscript "p" indicates that the current point of the grid is considered; (u_p and θ_p) are the theoretical surface Gaussian coordinates that are known for each grid point; $d_j^{(0)}$ $(j = 1, \ldots, m)$ represent the initial theoretical machine-tool settings; $\mathbf{n}_{mp}$ is the unit normal at the current grid point; $\mathbf{R}^{\star}_{mp} = (X^{\star}_{mp}, Y^{\star}_{mp}, Z^{\star}_{mp})$ is obtained from the measurements. Henceforth, we will assume that both surfaces have the same direction of the normal.

Equations (6.1) and (6.2) yield

$$a = (\boldsymbol{\rho}_{mp} - \mathbf{r}_{mp}) \cdot \mathbf{n}_{mp} \tag{6.3}$$

$$\lambda_p = (\mathbf{R}^{\star}_{mp} - \mathbf{r}_{mp}) \cdot \mathbf{n}_{mp} \tag{6.4}$$

The deviation of the real tooth surface $\Sigma^{\star}_m$ from the theoretical surface Σ_m is measured along the normal to the theoretical surface and can be represented as

$$\triangle b_p = \lambda_p - a = (\mathbf{R}^{\star}_{mp} - \boldsymbol{\rho}_{mp}) \cdot \mathbf{n}_{mp} \tag{6.5}$$

Taking into account equations (6.4) and (6.5) we obtain that

$$\triangle b_p = \lambda_p - a = (X^{\star}_{mp} - X_{mp}) \cdot n_{xmp} + (Y^{\star}_{mp} - Y_{mp}) \cdot n_{ymp} + (Z^{\star}_{mp} - Z_{mp}) \cdot n_{zmp} \quad (p = 1, \ldots, 45) \tag{6.6}$$

where, the subscript p is the index of a measured point; $(X^{\star}_{mp}, Y^{\star}_{mp}, Z^{\star}_{mp})$ are the coordinates of the center of the probe obtained by measurements; $(X_{mp}(u_p, \theta_p), Y_{mp}(u_p, \theta_p), Z_{mp}(u_p, \theta_p))$ are the

cartesian coordinates of the center of the probe for surface $\Sigma_{e,m}$ that is equidistant to the theoretical surface Σ_m that are represented in S_m; $n_{xmp}(u_p, \theta_p), n_{ymp}(u_p, \theta_p)$ and $n_{zmp}(u_p, \theta_p)$ are the projections in S_m of the unit theoretical surface normal. Surface parameters (u_p, θ_p) are considered as known for each point of measurements.

CHAPTER 7

MATHEMATICAL ASPECTS OF MINIMIZATION

Basic considerations

We consider two steps for computerized minimization of deviations of real tooth surfaces [9]:

(1). development of relations between corrections of machine-tool settings and surface deviations;

(2). minimization of deviations.

Step 1.: Variation of Tooth Surface Caused by Change of Machine-Tool Settings

The gear and the pinion tooth surface in accordance to expressions (2.4) are represented in S_m as follows,

$$\mathbf{r}_m = \mathbf{r}_m(u, \theta, d_j) \quad ; \quad \mathbf{n}_m = \mathbf{n}_m(u, \theta, d_j) \tag{7.1}$$

In equations (7.1), the tooth surface is represented in terms of surface coordinates u and θ. For simplicity, the subscript "m" is dropped in the following derivations. The first order variations of the surface that is caused by the change of machine-tool settings and surface coordinates is represented as

$$\delta \mathbf{r} = \frac{\partial \mathbf{r}}{\partial \theta}\delta\theta + \frac{\partial \mathbf{r}}{\partial u}\delta u + \sum_{j=1}^{m} \frac{\partial \mathbf{r}}{\partial d_j}\delta d_j \tag{7.2}$$

where, m is the number of machine-tool settings.

We multiply both sides of equation (7.2) by the surface unit normal $\mathbf{n}$ and take into account that $\frac{\partial \mathbf{r}}{\partial \theta} \cdot \mathbf{n} = \frac{\partial \mathbf{r}}{\partial u} \cdot \mathbf{n} = 0$ since $\frac{\partial \mathbf{r}}{\partial \theta}$ and $\frac{\partial \mathbf{r}}{\partial u}$ lie in the plane that is tangent to the surface. The surface normal variations can be found as

$$\delta \mathbf{r} \cdot \mathbf{n} = \sum_{j=1}^{m} (\frac{\partial \mathbf{r}}{\partial d_j} \cdot \mathbf{n})\delta d_j \tag{7.3}$$

Step 2.: Linear Equations

The surface normal variations must be equal to the deviations obtained by measurements. Thus we will obtain an overdetermined system of n linear equations in m unknowns (m is equal to the number of machine-tool settings) represented as

$$\sum_{j=1}^{m} (\frac{\partial \mathbf{r}_p}{\partial d_j} \cdot \mathbf{n}_p)\delta d_j = \sum_{j=1}^{m} a\delta d_j = \triangle b_p \qquad (p = 1, \ldots, n) \tag{7.4}$$

where, subscript p is the index of a measured point.

The number n of equations is equal to the number of points for measurements. In this report, the number n is equal to 45 as mentioned in chapter 4

We can now consider a system of n linear equations in m unknowns ($m \ll n$) of the following structure

$$\left.\begin{array}{l} a_{11}\delta d_1 + a_{12}\delta d_2 + \ldots + a_{1m}\delta d_m = \triangle b_1 \\ a_{21}\delta d_1 + a_{22}\delta d_2 + \ldots + a_{2m}\delta d_m = \triangle b_2 \\ \ldots\ldots\ldots\ldots\ldots\ldots\ldots\ldots\ldots\ldots\ldots\ldots \\ \ldots\ldots\ldots\ldots\ldots\ldots\ldots\ldots\ldots\ldots\ldots\ldots \\ a_{n1}\delta d_1 + a_{n2}\delta d_2 + \ldots + a_{nm}\delta d_m = \triangle b_n \end{array}\right\} \qquad (7.5)$$

Here:

$$\triangle b_p = (\mathbf{R}^{\star}_{mp} - \boldsymbol{\rho}_{mp}) \cdot \mathbf{n}_{mp} \qquad (p = 1, \ldots, n) \qquad (7.6)$$

where subscript p is the index of a measured point; a_{pj} $(p = 1, \ldots, n; j = 1, \ldots, m)$ represent the dot product of partial derivatives $\dfrac{\partial \mathbf{r}_p}{\partial d_j}$ and unit normal $\mathbf{n}_p$ $(p = 1, \ldots, n \;\; ; \;\; j = 1, \ldots, m)$.

The system (7.5) of linear equations is overdetermined since $m \ll n$. The mathematical aspect of the problem for the minimization of deviations is the determination of such unknowns δd_j $(j = 1, \ldots, m)$ that will minimize the difference between the left and right sides of equations (7.5). One of the widely used methods for the solution of the overdetermined system of linear equations is the least-square method. In this work we have used a commercially available subroutine DLSQRR of IMSL MATH/LIBRARY [7] for computerization of the procedure.

Part II

APPLICATIONS TO COORDINATE MEASUREMENTS OF HYPOID PINIONS AND GEARS

CHAPTER 8

Minimization Of Deviations of Face-Milled Hypoid Formate Gear

8.1 Equations of Theoretical Tooth Surface Σ_2

The head-cutter is provided with inner and outer straight-lined blades as it is shown in Fig. 8.1. The blades that are rotated about the axis of the head-cutter generate two cones. Each tooth side of formate face-hobbed gear is generated by a cone and the gear tooth surface is the surface of the generating cone. The angular velocity of rotation of blades is not related with the process of surface generation but depends only on the desired velocity of cutting. Usually, the formate gear of a hypoid drive is cut by the duplex method [8,9]. This means that both sides of the gear space are generated simultaneously by a head cutter and the machine tool settings are the same for both sides.

Both generating cones (Fig. 8.2) can be represented by the same equation given as

$$\mathbf{r}_c = \begin{bmatrix} -s_G \cos\alpha_G \\ (r_G - s_G \sin\alpha_G)\sin\theta_G \\ (r_G - s_G \sin\alpha_G)\cos\theta_G \end{bmatrix} \tag{8.1}$$

Here: $\mathbf{r}_c$ is the position vector; $r_G = r_G^{(i)}$ is the cutter tip radius; $s_G = s_G^{(i)}$, $\alpha_G = \alpha_G^{(i)}$, (i=1,2); $s_G^{(i)}$ and $\alpha_G^{(i)}$ are negative for concave side , and positive for convex side ($i = 1, 2$ for concave and convex

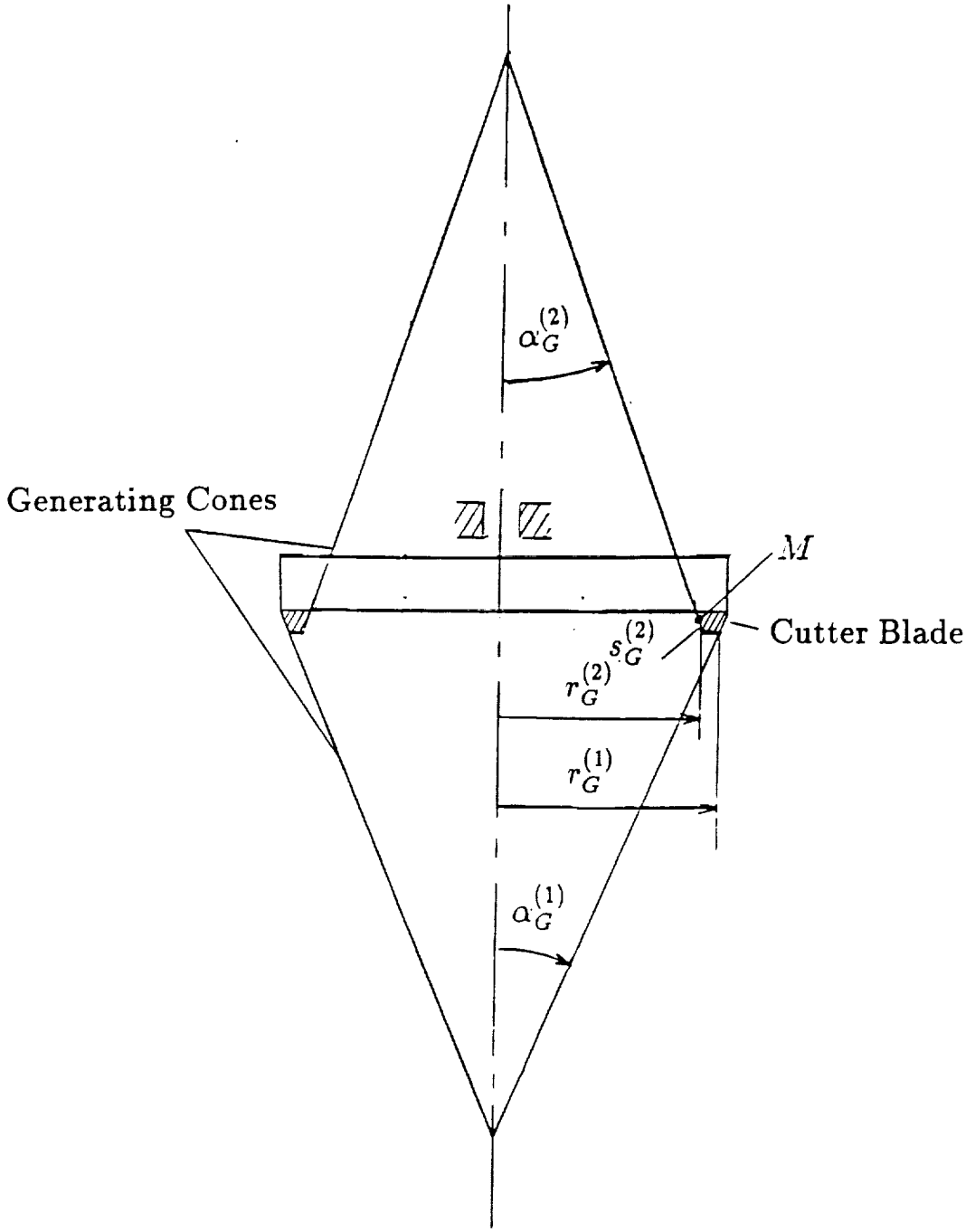

Figure 8.1: Head Cutter for Tooth Surface Generation

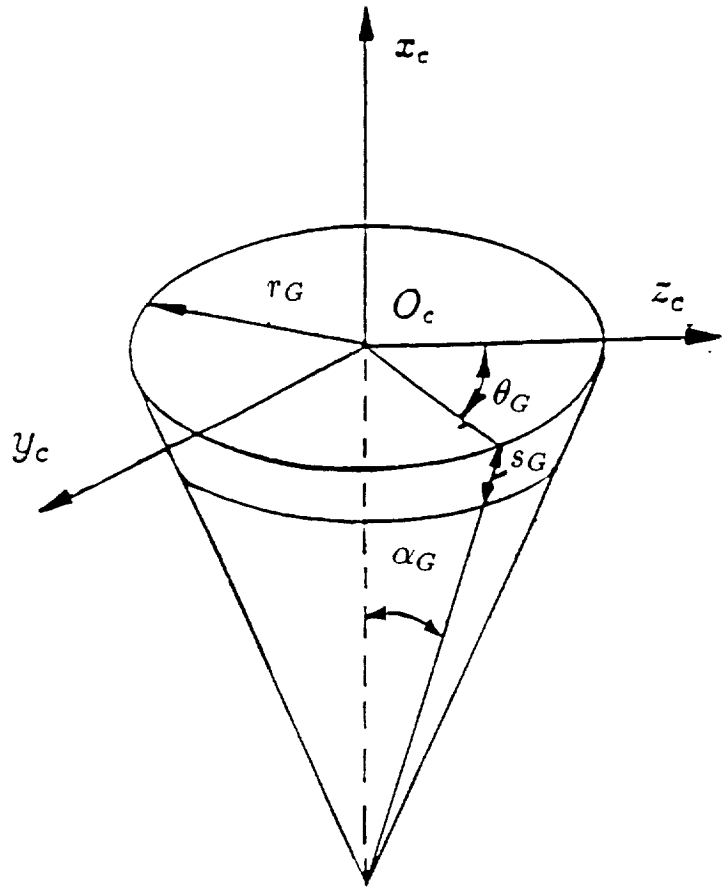

Figure 8.2: Generating Cone Coordinate System

side, respectively). Parameters s_G and θ_G represent the Gaussian coordinates of the generating surface. The unit normal to the generating surface is represented by the equations

$$\mathbf{N}_c = \frac{\partial \mathbf{r}_c}{\partial s_G} \times \frac{\partial \mathbf{r}_c}{\partial \theta_G} \quad ; \qquad \mathbf{n}_c = \frac{\mathbf{N}_c}{|\mathbf{N}_c|} = \begin{bmatrix} \sin\alpha_G \\ -\cos\alpha_G \sin\theta_G \\ -\cos\alpha_G \cos\theta_G \end{bmatrix} \tag{8.2}$$

Fig. 8.3 shows the installment of the head-cutter (generating cone) and the gear on the cutting machine. Coordinate systems S_o, S_c and S_2 are rigidly connected to the cutting machine, the head-cutter and the being generated gear, respectively. In the process of generation, all three coordinate systems do not perform relative motions with respect to each other since the gear is formate cut. Thus we may consider that they are rigidly connected each to other. The generated gear tooth surface is the same as the surface of the generating cone for this type of gear. The installment of the head cutter is determined with machine-settings H_2 and V_2 that represent the location of origin O_c of coordinate system S_c in S_o. The installment of the gear on the cutting machine is represented by settings $\gamma_m^{(2)}$ and ΔX_m. The origin O_2 of coordinate system S_2 coincides with the point of intersection of the shortest distance of the hypoid gear drive with the gear axis (i.e., crossing point). Parameter ΔX_m represents the location of O_2 with respect to O_0 -the origin of S_o. Parameter $\gamma_m^{(2)}$ represents the orientation of gear axis in plane $y_o = 0$. The set of parameters H_2, V_2, ΔX_m, and $\gamma_m^{(2)}$ represents the set of the to-be corrected settings for minimization of deviations of real gear tooth surfaces. The theoretical gear tooth surface Σ_2 and the surface unit normal are represented in S_2 by using the following matrix equations

$$\mathbf{r}_2(s_G, \theta_G, d_j) = [M_{2c}]\mathbf{r}_c(s_G, \theta_G) = [M_{2o}][M_{oc}]\mathbf{r}_c(s_G, \theta_G) \tag{8.3}$$

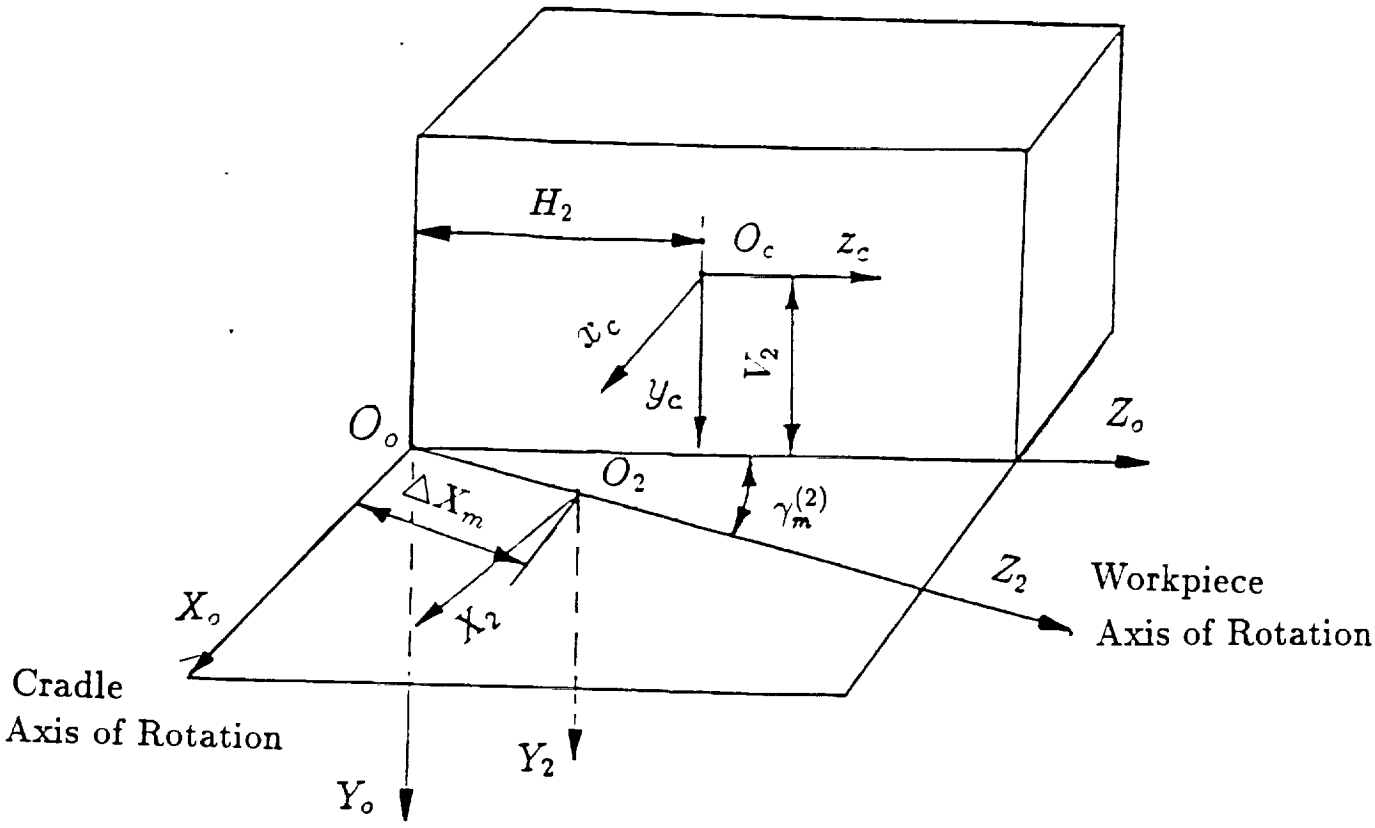

Figure 8.3: Installment of the Head Cutter with respect to Machine and Workpiece.
(For Formate Manufacture There Is No Rotation About Cradle Axis x_o or Workpiece Axis z_2)

$$[M_{2o}] = \begin{bmatrix} \cos\gamma_m^{(2)} & 0 & -\sin\gamma_m^{(2)} & 0 \\ 0 & 1 & 0 & 0 \\ \sin\gamma_m^{(2)} & 0 & \cos\gamma_m^{(2)} & -\triangle X_m \\ 0 & 0 & 0 & 1 \end{bmatrix} \tag{8.4}$$

$$[M_{oc}] = \begin{bmatrix} 1 & 0 & 0 & 0 \\ 0 & 1 & 0 & -V_2 \\ 0 & 0 & 1 & H_2 \\ 0 & 0 & 0 & 1 \end{bmatrix} \tag{8.5}$$

$$\mathbf{n}_2(\theta_G) = [L_{2c}][n_c] = [L_{2o}][L_{oc}]\mathbf{n}_c(\theta_G) \tag{8.6}$$

$$[L_{2o}] = \begin{bmatrix} \cos\gamma_m^{(2)} & 0 & -\sin\gamma_m^{(2)} \\ 0 & 1 & 0 \\ \sin\gamma_m^{(2)} & 0 & \cos\gamma_m^{(2)} \end{bmatrix} \tag{8.7}$$

$$[L_{oc}] = \begin{bmatrix} 1 & 0 & 0 \\ 0 & 1 & 0 \\ 0 & 0 & 1 \end{bmatrix} \tag{8.8}$$

Equations from (8.1) to (8.8) enable the determination of the theoretical gear tooth surface Σ_2 and its unit normal as (2.4),

$$\mathbf{r}_2(s_G, \theta_G; d_j) \in C^2 \quad (j = 1, \ldots, 4)\ ; s_G, \theta_G \in E\ ; \quad \mathbf{n}_2(\theta_G, \gamma_m^{(2)}) \neq 0 \tag{8.9}$$

Here d_j are the machine-tool settings $\triangle X_m, H_2, V_2$ and $\gamma_m^{(2)}$. The Gaussian surface coordinates are designated by s_G and θ_G.

We will also need the parametric representation of a surface $\Sigma_{(e)2}$ that is equidistant to the theoretical surface Σ_2. Such a surface is represented as (4.2),

$$\rho_2 = \mathbf{r}_2(s_G, \theta_G) + a\mathbf{n}_2(\theta_G) \tag{8.10}$$

where a is the radius of the ball surface of the probe.

8.2 Determination and Minimization of Deviations

After the theoretical tooth surface Σ_2 of hypoid gear are obtained, the deviations of the real surface from the theoretical one and minimized the deviations by corrections of the previous applied machine-tool settings can be determined in chapter 6 and 7. Both sides of a formate cut gear tooth are generated simultaneously (by duplex method), and the machine-tool settings are the same for both sides. Therefore the minimization of deviations for both side surfaces of the tooth must be obtained by the appropriate change of the same machine-tool settings.

Computational Procedure

The computational procedure is similar to that we discussed in Part I as follows:

Step 1. Create grid points on the to-be measured surface that are chosen as points of contact between the tooth surface and the probe (in chapter 4).

Step 2. Determine the reference point in coordinate system S_m (in chapter 4).

Step 3. Determine the deviations of real tooth surface from equation (6.6).

Step 4. Minimize the deviations from equation (7.4).

8.3 Results of Coordinate Measurements and Minimization of Deviations for Hypoid Gears

The numerical example is based on the experiment that has been performed at the Dana Corporation (Fort Wayne, USA). The deviations of real gear tooth surfaces for both sides of the gear tooth have been obtained by measurements on the Zeiss machine. The developed approach has been used for minimization of obtained deviations. The number of measured points is $p = 90$ of both sides of the tooth ($p = 1, \ldots, 45$ for convex side ; $p = 46, \ldots, 90$ for concave side). Fig. 8.4 and Fig. 8.5 illustrate the deviations $\triangle b_p$ of the real surface from the theoretical one for the driving side and coast side, respectively. The input data, original machine-tools settings, the corrections of machine-tool settings and the corrected machine-tool settings are shown in Table A.1 in Appendix. The experimental data include the coordinates of theoretical surface, the projections of surface unit normal, and coordinates of the real surface (obtained by measurements) are represented in Table A.2-A.7 in Appendix. Based on the corrected machine-tool settings, we can create a new surface which will optimally fit the theoretical surface after the surface is distorted by heat-treatment during manufacture. The minimized deviations between the new surface and the theoretical surface are shown in Fig. 8.6.

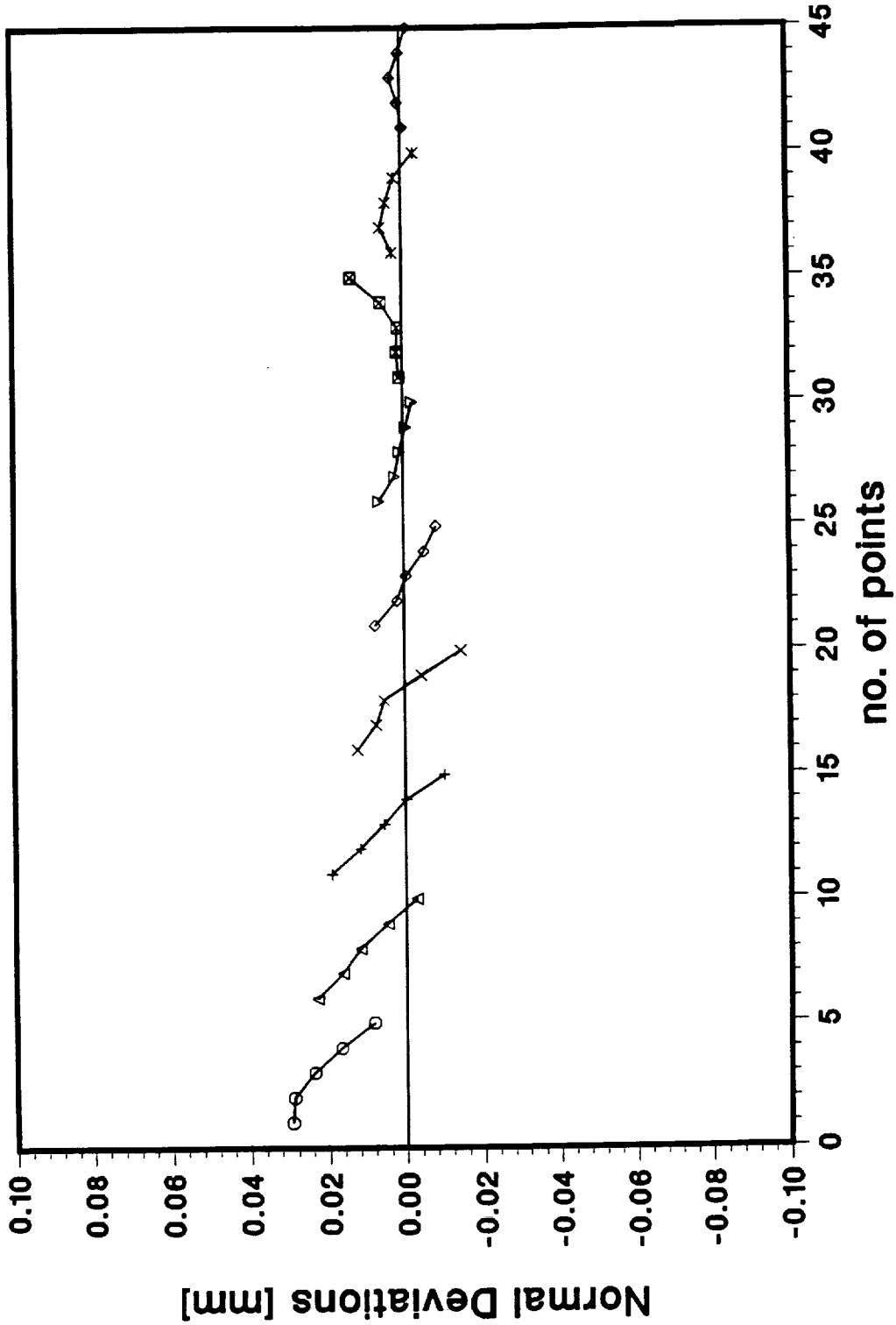

Figure 8.4: Deviations of Gear Real Tooth Surface (Driving Side)

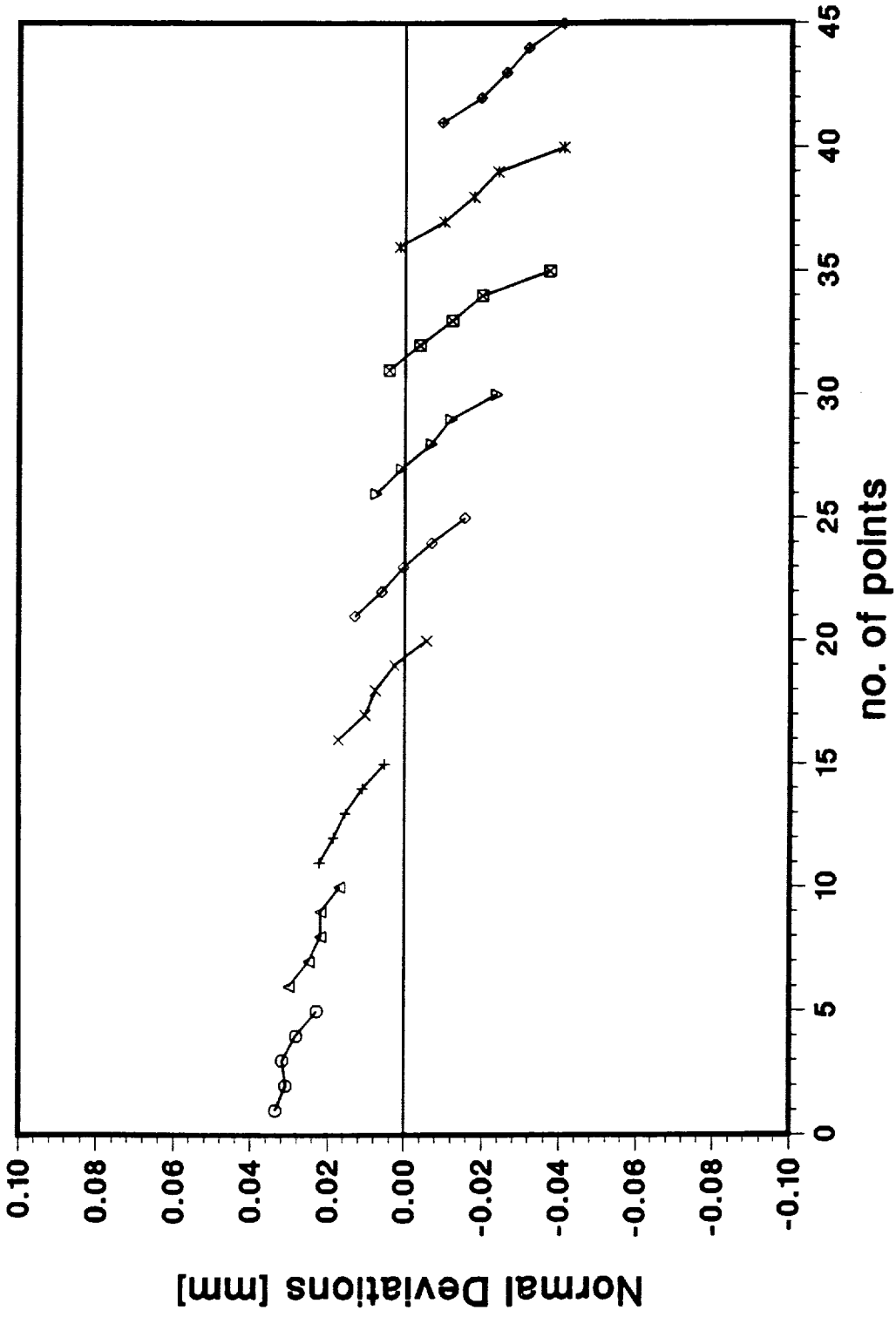

Figure 8.5: Deviations of Gear Real Tooth Surface (Coast Side)

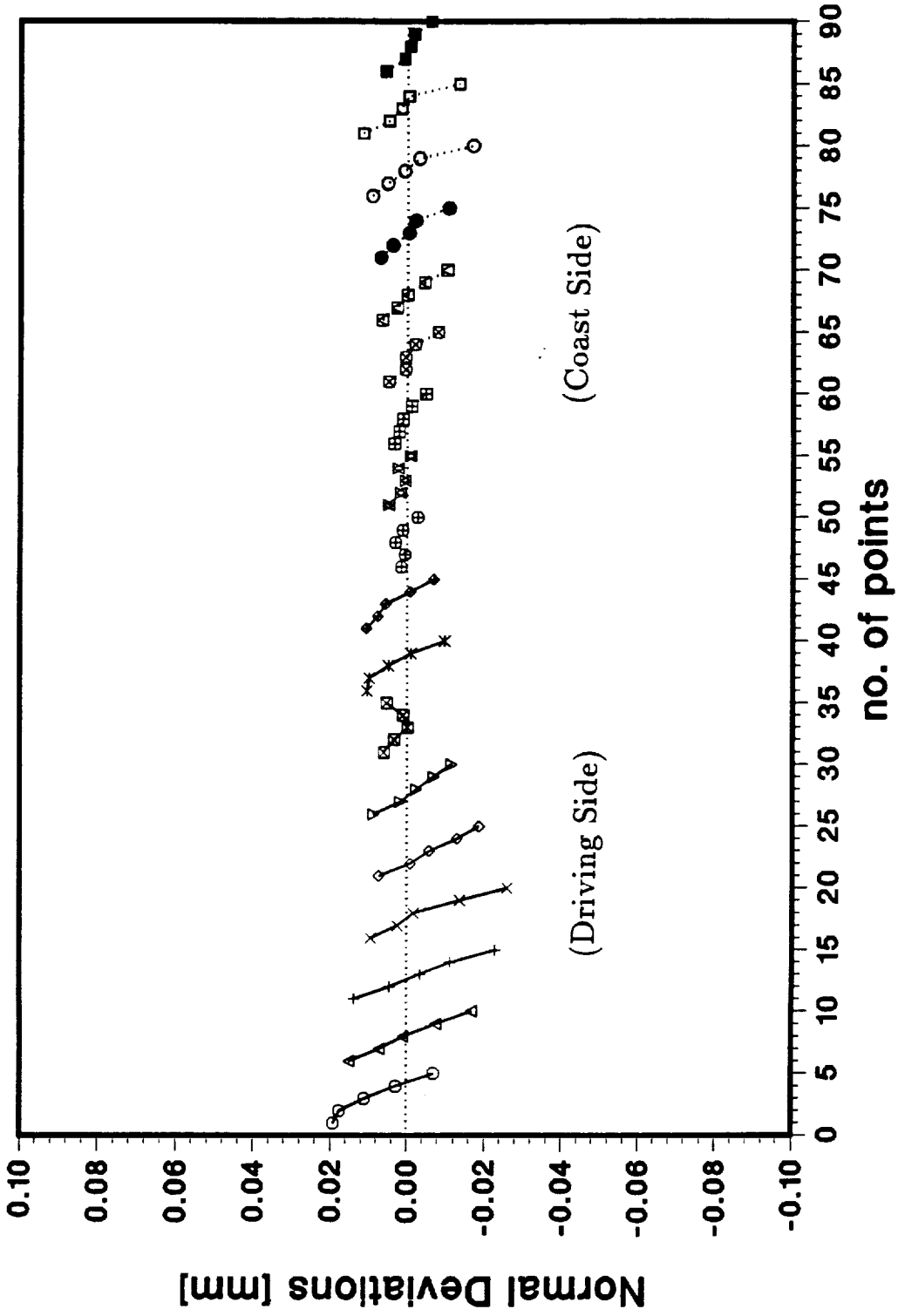

Figure 8.6: Minimized Deviations

CHAPTER 9

Minimization Of Deviations of Face-Milled Hypoid Pinion

9.1 Generation of Pinion Theoretical Tooth Surface Σ_1

The pinion tooth surface is generated as the envelope to the family of tool cone surfaces. The derivation of the generated pinion tooth surface is based on ideas that have been represented in reference [3,10].

Coordinate Systems

Henceforth, we will consider the following coordinate systems: (i) the fixed ones, $S_{0'}(x_{0'}, y_{0'}, z_{0'})$ and $S_q(x_q, y_q, z_q)$ that are rigidly connected to the cutting machine (Fig. 9.1 and Fig. 9.2), and (ii) the movable coordinate systems $S_{c'}$ and S_1 that are rigidly connected to the cradle of cutting machine and the pinion, respectively. The origin, O_1, of coordinate system S_1 coincides with the point of intersection of the shortest distance of the hypoid gear drive with the pinion axis (i.e., crossing point). In the process of generation the cradle with $S_{c'}$ performs rotational motion about the $z_{o'}$-axis with angular velocity $\omega^{(c)}$ and the pinion with S_1 performs rotational motion about the x_q-axis with angular velocity $\omega^{(p)}$ (Fig. 9.2).

The tool (the head-cutter) is mounted on the cradle and performs rotational motion with the cradle. Coordinate system S_t is rigidly connected to the cradle. To describe the installment of the tool with respect to the cradle we use coordinate system S_b (Fig. 9.1 and Fig. 9.3).

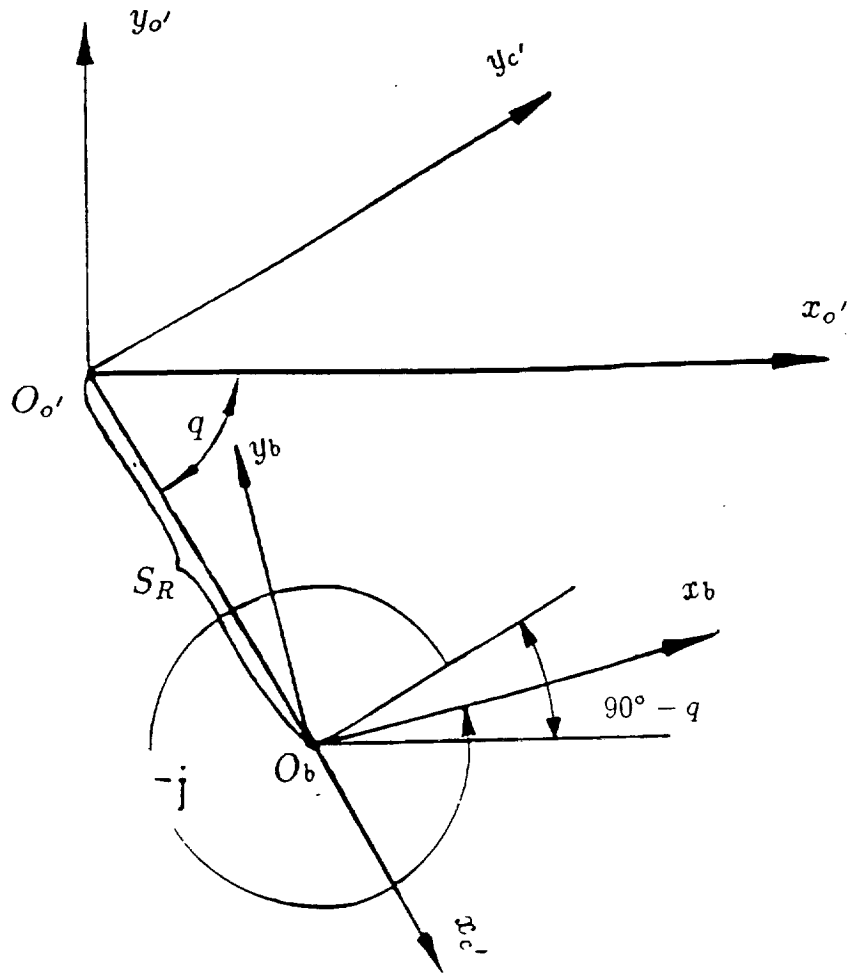

Figure 9.1: Cutting Machine and Cradle Coordinate Systems

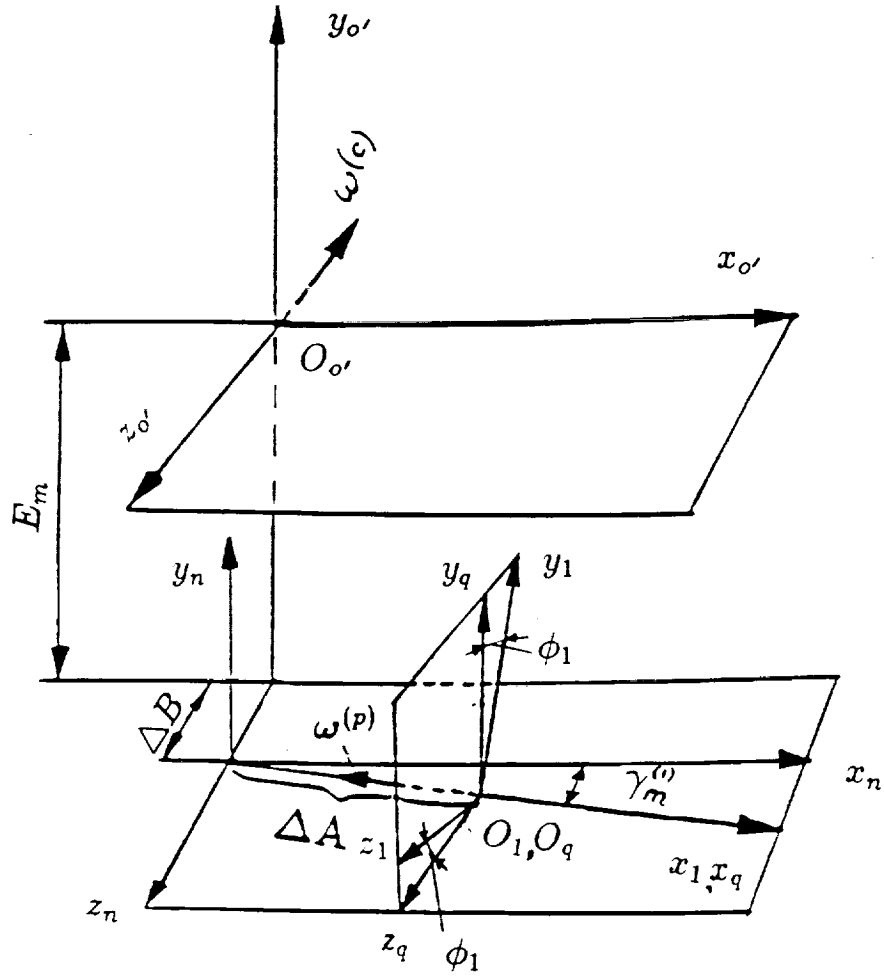

Figure 9.2: Angular Velocities of Cradle and Pinion

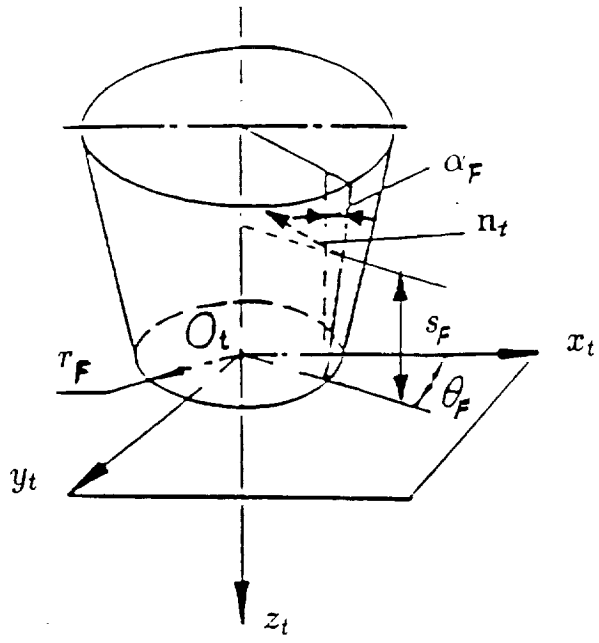

(a) Head-Cutter Surface Parameters

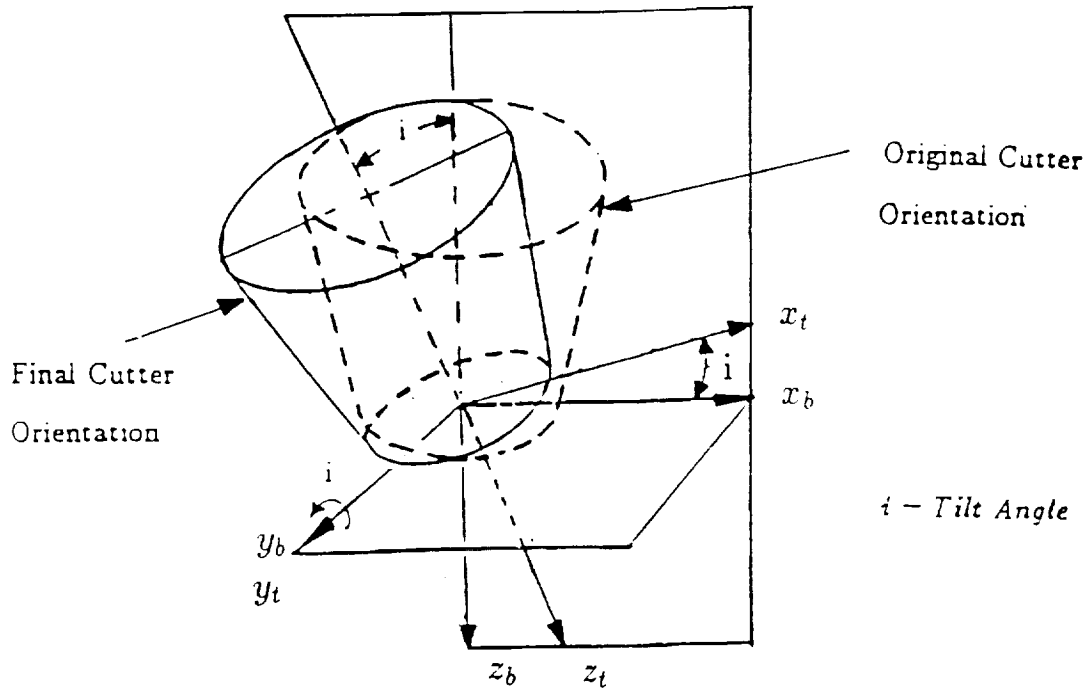

(b) Coordinate Systems for Head-Cutter Tilt

Figure 9.3: Pinion Head-Cutter Surface

The required orientation of the head-cutter with respect to the cradle [4] is accomplished as follows:

(i) coordinate systems S_b and S_t are rigidly connected and then they are turned as one rigid body about the $z_{c'}$-axis through the swivel angle j (Fig. 9.1);

(ii) then the head-cutter with coordinate system S_t is tilted about the y_b-axis under the angle i (Fig. 9.3.b)). The head-cutter is rotated about its axis z_t but the angular velocity in this motion is not related with the generation process and depends only on the desired velocity of cutting.

It will be shown below that the deviations of real pinion tooth surface can be minimized by corrections of parameters of installment of the pinion and the head-cutter. These pinion setting parameters are E_m– the machine offset, $\gamma_m^{(1)}$– the machine-root angle, $\triangle B$– the sliding base, $\triangle A$– the machine center to back (Fig. 9.2). The head-cutter settings parameters are: S_R– radial setting, θ_c– initial value of cradle angle, j– the swivel angle (Fig. 9.1) , and i– the tilt angle (Fig. 9.3.b).

9.2 Equations of Theoretical Tooth Surface

Tool Surface Equations:

The head-cutter surface is a cone and is represented in S_t (Fig. 9.3) as

$$\mathbf{r}_t(s_F, \theta_F) = \begin{bmatrix} (r_F + s_F \sin\alpha_F)\cos\theta_F \\ (r_F + s_F \sin\alpha_F)\sin\theta_F \\ -s_F \cos\alpha_F \\ 1 \end{bmatrix} \tag{9.1}$$

Here: (s_F, θ_F) are the Gaussian surface coordinates, α_F is the blade angle and r_F is the cutter

point radius. Vector function (9.1) with α_F positive and α_F negative represents surfaces of two head-cutter that are used to cut the pinion concave side and convex side, respectively (Fig. 9.4).

The unit normal to the head-cutter surface is represented in S_t by the equations

$$\mathbf{n}_t = \begin{bmatrix} -\cos\alpha_F \cos\theta_F \\ -\cos\alpha_F \sin\theta_F \\ -\sin\alpha_F \end{bmatrix} \tag{9.2}$$

Family of Tool Surfaces

The cradle with the mounted head-cutter and the pinion perform rotational motions about the axes-$z_{o'}$ and x_q, respectively. The angles of cradle and pinion rotation, q and ϕ_1 are related by the equation

$$q = \theta_c + m_{cp}\phi_1 \tag{9.3}$$

Here: θ_c is the initial value of cradle angle and $m_{cp} = \dfrac{\omega^{(c)}}{\omega^{(p)}}$ is the gear cutting ratio.

The family of tool surfaces is generated in S_1 and this family is represented by the matrix equation

$$\mathbf{r}_1(s_F, \theta_F, \phi_1) = [M_{1q}(\phi_1)][M_{qn}][M_{no'}][M_{o'c'}][M_{c'b}][M_{bt}]\mathbf{r}_t(s_F, \theta_F) \tag{9.4}$$

Coordinate system S_n is an auxiliary fixed coordinate system whose axes are parallel to axes of $S_{o'}$ (Fig. 9.2). Matrices in equation (9.4) are represented as follows

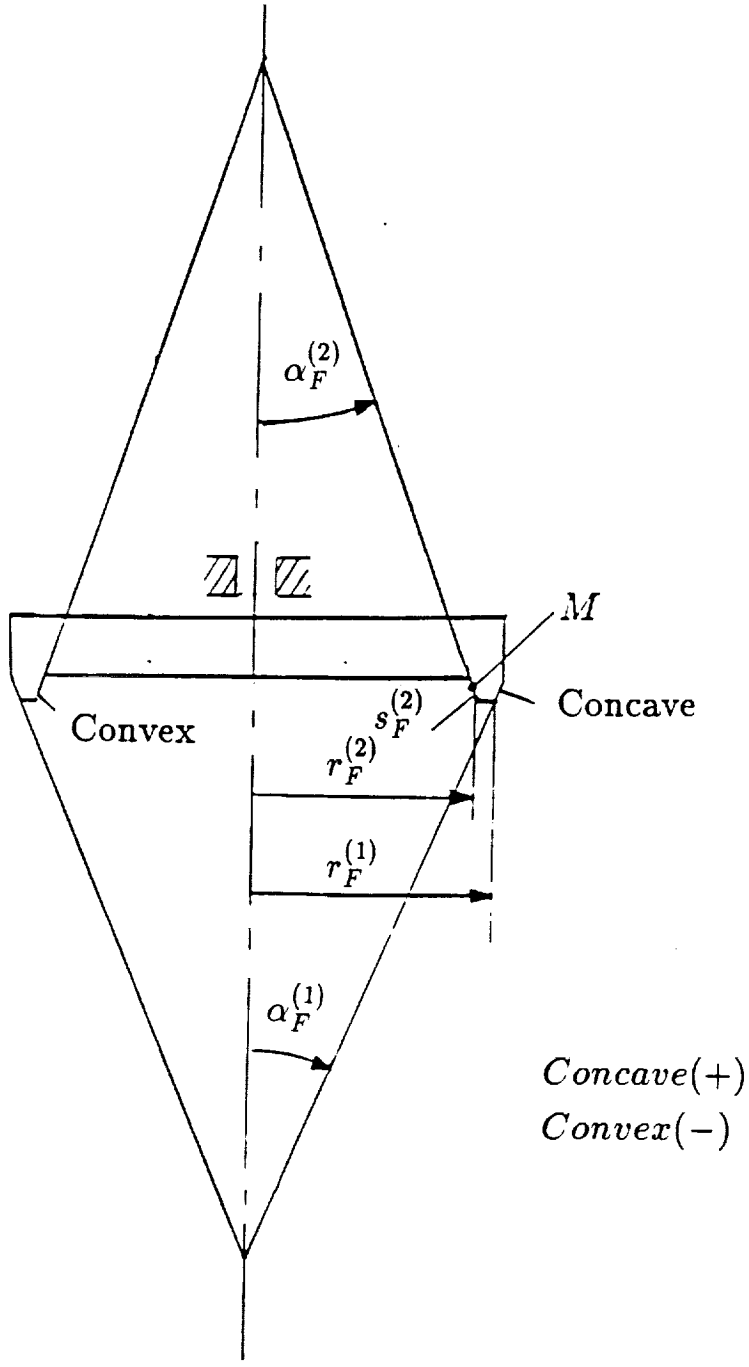

Figure 9.4: Head-Cutter Showing Point Radii and Blade Angles

$$[M_{bt}] = \begin{bmatrix} \cos i & 0 & \sin i & 0 \\ 0 & 1 & 0 & 0 \\ -\sin i & 0 & \cos i & 0 \\ 0 & 0 & 0 & 1 \end{bmatrix} \tag{9.5}$$

$$[M_{c'b}] = \begin{bmatrix} -\sin j & -\cos j & 0 & S_R \\ \cos j & -\sin j & 0 & 0 \\ 0 & 0 & 1 & 0 \\ 0 & 0 & 0 & 1 \end{bmatrix} \tag{9.6}$$

$$[M_{o'c'}] = \begin{bmatrix} \cos q & \sin q & 0 & 0 \\ -\sin q & \cos q & 0 & 0 \\ 0 & 0 & 1 & 0 \\ 0 & 0 & 0 & 1 \end{bmatrix} \tag{9.7}$$

$$[M_{no'}] = \begin{bmatrix} 1 & 0 & 0 & 0 \\ 0 & 1 & 0 & E_m \\ 0 & 0 & 1 & -\triangle B \\ 0 & 0 & 0 & 1 \end{bmatrix} \tag{9.8}$$

$$[M_{qn}] = \begin{bmatrix} \cos \gamma_m^{(1)} & 0 & \sin \gamma_m^{(1)} & -\triangle A \\ 0 & 1 & 0 & 0 \\ -\sin \gamma_m^{(1)} & 0 & \cos \gamma_m^{(1)} & 0 \\ 0 & 0 & 0 & 1 \end{bmatrix} \tag{9.9}$$

$$[M_{1q}] = \begin{bmatrix} 1 & 0 & 0 & 0 \\ 0 & \cos\phi_1 & \sin\phi_1 & 0 \\ 0 & -\sin\phi_1 & \cos\phi_1 & 0 \\ 0 & 0 & 0 & 1 \end{bmatrix} \tag{9.10}$$

Matrix equation (9.4) and tool surface equation (9.1) represent in S_1 the family of tool surfaces in the form

$$\mathbf{r}_1 = \mathbf{r}_1(s_F, \theta_F, \phi_1) \tag{9.11}$$

Equation of Meshing

The pinion tooth surface generated in S_1 is the envelope to the family of tool surfaces. To determine such an envelope we have to derive the equation of meshing [3] by using the equation

$$\mathbf{n}^{(p)} \cdot \mathbf{v}^{(cp)} = \mathbf{N}^{(p)} \cdot \mathbf{v}^{(cp)} = f(s_F, \theta_F, \phi_1) = 0 \tag{9.12}$$

where $\mathbf{n}^{(p)}$ and $\mathbf{N}^{(p)}$ are the unit normal and the normal to the tool surface, and $\mathbf{v}^{(cp)}$ is the velocity in relative motion.

Equation (9.12) is invariant with respect to the coordinate system where the vectors of the scalar product are represented. Representing those vectors in $S_{o'}$, we can derive the equation of meshing using the following procedure

Step 1.: Vector $\mathbf{n}_{o'}$ can be represented as

$$\mathbf{n}_{o'} = [L_{o'c'}][L_{c'b}][L_{bt}]\mathbf{n}_t \tag{9.13}$$

where [L] is the 3×3 submatrix of [M]. The superscript in $\mathbf{n}_{o'}^{(p)}$ is dropped for simplification of designations.

Step 2.: The sliding velocity $\mathbf{v}_{o'}^{(cp)}$ (see [3]) is represented by (Fig. 9.2):

$$\mathbf{v}_{o'}^{(cp)} = [(\boldsymbol{\omega}^{(c)} - \boldsymbol{\omega}^{(p)}) \times \mathbf{r}_{o'}] + (\overline{O_{o'A}} \times \boldsymbol{\omega}^{(p)}) \tag{9.14}$$

Here:

$$\mathbf{r}_{o'} = [M_{o'c'}][M_{c'b}][M_{bt}]\mathbf{r}_t \tag{9.15}$$

$$\overline{O'_oA} = [0 \quad -E_m \quad \triangle B]^T \tag{9.16}$$

$$\boldsymbol{\omega}^{(p)} = -[\cos\gamma_m^{(1)} \quad 0 \quad \sin\gamma_m^{(1)}]^T \quad ; \quad (|\boldsymbol{\omega}^{(p)}| = 1) \tag{9.17}$$

$$\boldsymbol{\omega}^{(c)} = -[0 \quad 0 \quad m_{cp}] \tag{9.18}$$

Equations (9.12), (9.13) and (9.14) yield the equation of meshing in form

$$f(s_F, \theta_F, \phi_1) = 0 \tag{9.19}$$

Pinion Tooth Surface Equations

The pinion tooth surface equations are represented in three-parametric form by the equations

$$\mathbf{r}_1(s_1, \theta_F, \phi_1) = [M_{1t}]\mathbf{r}_t(s_F, \theta_F) \qquad f(s_F, \theta_F, \phi_1) = 0 \tag{9.20}$$

However, since equations (9.20) are linear with respect to the Gaussian coordinate s_F we can eliminate s_F and represent the pinion tooth surface in two-parametric form as

$$\mathbf{r}_1(\theta_F, \phi_1, d_j)\epsilon C^2 \qquad (\theta_F, \phi_1)\epsilon E \tag{9.21}$$

Here: d_j $(j = 1, \ldots, 8)$ designate the installment parameters; $E_m, \gamma_m^{(1)}, \triangle B, \triangle A, S_R, \theta_c, j$ and i ; C^2 designates that the vector function has derivatives on arguments θ_F and ϕ_1 at least of the first and second order.

The normal to the pinion tooth surface is represented as

$$\mathbf{n}_1(\theta_F, \phi_1, d_k) \tag{9.22}$$

where d_k $(k = 1,2,3,4)$ designate the installment parameters $\gamma_m^{(1)}, \theta_c, j$ and i.

9.3 The Grid

We recall that the grid (Fig. 4.1) is a set of points on the theoretical surface Σ that are chosen as points of contact between the tooth surface and the probe.

The development of the grid is based on the following considerations (see chapter 4):

(1). In accordance to the practice of measurements a set of 45 points is usually chosen for the measurements that are located in nine longitudinal sections of the pinion surface with five points in each section (Fig. 4.3).

(2). Mean point M (Fig. 4.3 and Fig. 9.5) of the theoretical surface Σ is usually chosen as the *reference* point, that is necessary for the initial installment of the probe on the coordinate measurement machine. Obviously, the real tooth surface Σ^* does not pass through M and the surface normal at M intersects the real surface at M^*. We can consider that an imaginary theoretical surface $\Sigma_{(e)}$ that is equidistant to Σ passes through M^* and the deviations of the real surface are determined with respect to $\Sigma_{(e)}$.

As shown in Fig. 9.5 the position of the mean point M can be represented in S_1 by XL and RL, which are determined by the following equations

$$\left.\begin{aligned} XL &= A\cos\Gamma_1 + (b_G - \frac{h_m}{2})\sin\Gamma_1 \\ RL &= A\sin\Gamma_1 - (b_G - \frac{h_m}{2})\cos\Gamma_1 \end{aligned}\right\} \tag{9.23}$$

Here, A is the mean cone distance; Γ_1 is the pinion pitch angle; b_G is the mean dedendum and h_m is the mean whole depth; XL and RL are measured along the pinion axis and perpendicular to this axis, respectively.

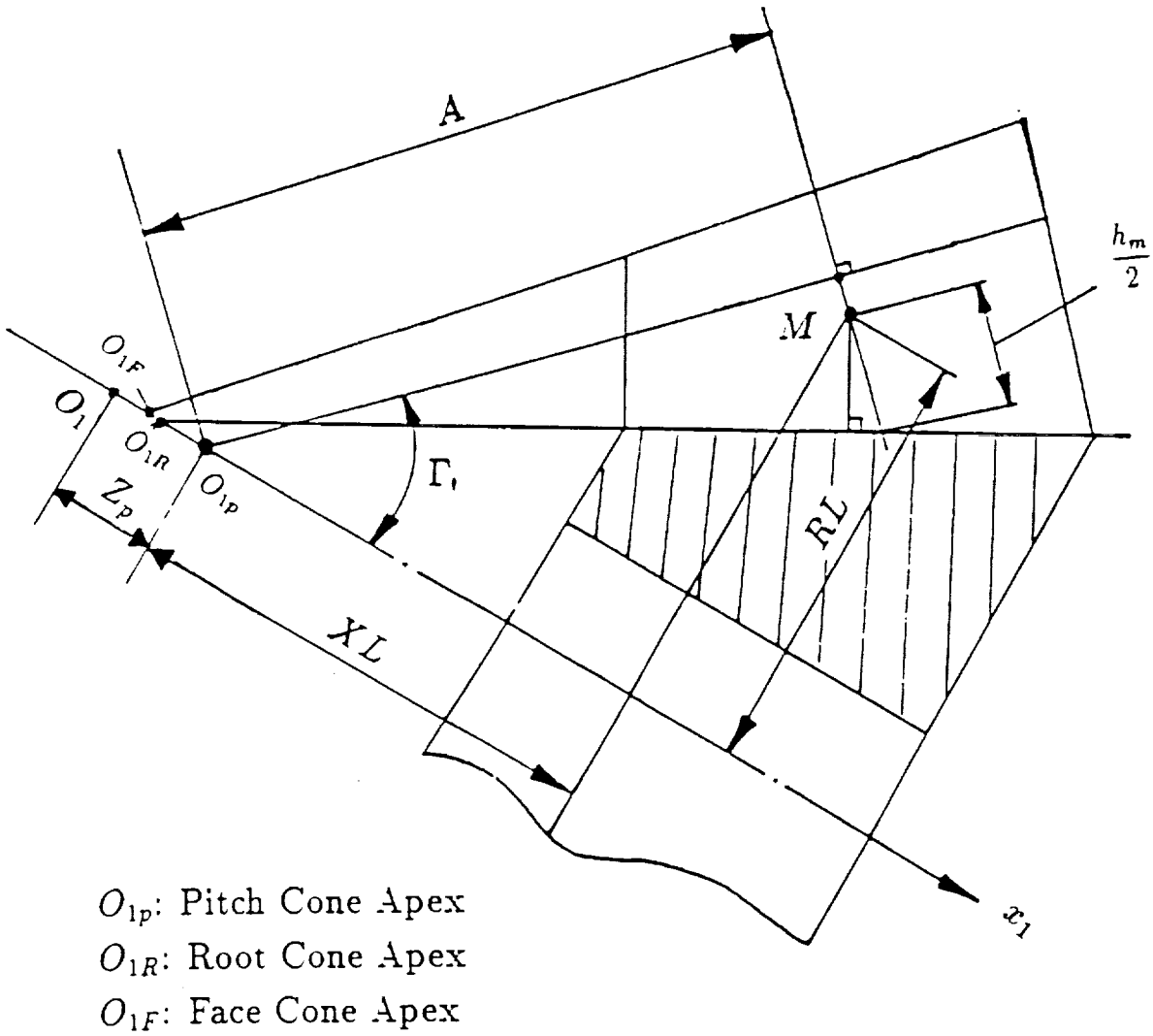

Figure 9.5: Mean Point

Combining equation (9.23) with surface equation (9.21), we may obtain two nonlinear equations in terms of $(\phi_1^{(o)}, \theta_F^{(o)})$,

$$\left.\begin{aligned} x_1(\phi_1^{(o)}, \theta_F^{(o)}) &= XL + Z_1 \\ y_1^2(\phi_1^{(o)}, \theta_F^{(o)}) + z_1^2(\phi_1^{(o)}, \theta_F^{(o)}) &= RL^2 \end{aligned}\right\} \tag{9.24}$$

Here, Z_p is the pitch cone apex beyond the crossing point O_1.

Solving equation system (9.24), we may determine surface coordinates $(\phi_1^{(o)}, \theta_F^{(o)})$ for the reference point and also its Cartesian coordinate $(x_1^{(o)}, y_1^{(o)}, z_1^{(o)})$.

(3). After the reference point is located, the rest of grid points can be chosen with the consideration that the grid points must be located uniformly on the working part of the tooth surface.

(4). Points on surface $\Sigma_{(e)1}$ that is equidistant to theoretical surface Σ_1 can be determined in S_1 with the vector equation

$$\boldsymbol{\rho}_1 = \mathbf{r}_1(\phi_1, \theta_F) + a\mathbf{n}_1(\phi_1, \theta_F) \tag{9.25}$$

where a is the radius of the ball surface of the probe. Equations (9.24) and (9.25) are represented in the terms of the Gaussian surface coordinates. Equations (9.25) represent in S_1 the surface that might be traced out by the center of the probe if the surface deviations are equal to zero.

9.4 Determination of Reference Point in Coordinate System S_m

We recall that coordinate system S_m is rigidly connected to the coordinate measurement machine and our purpose is to determine the initial installments of the pinion on the machine to provide the contact of the probe with the pinion mean surface point.

We consider that the pinion is installed with its back-face flush against the base plane of the CMM such that the origin of coordinate system S_m, O_m, coincides with O_1 and thus parameter l

is equal to zero (Fig. 9.6). Usually, the measurement process is performed in a coordinate system S_m where the y_m coordinate of the mean point is zero.

According to drawings of Fig. 9.7, the coordinate transformation from S_1 to S_m with $\cdot = 0$ is as follows,

$$[r_m] = [M_{m1}][r_1] = [M_{m1'}][M_{1'1}][r_1] \tag{9.26}$$

$$[M_{m1}] = [M_{m1'}][M_{1'1}] = \begin{bmatrix} 0 & -\sin\delta & -\cos\delta & 0 \\ 0 & -\cos\delta & \sin\delta & 0 \\ -1 & 0 & 0 & 0 \\ 0 & 0 & 0 & 1 \end{bmatrix} \tag{9.27}$$

Then we obtain for the reference point

$$\left.\begin{aligned} x_m &= -y_1\sin\delta - z_1\cos\delta \\ y_m &= -y_1\cos\delta + z_1\sin\delta \\ z_m &= -x_1 \end{aligned}\right\} \tag{9.28}$$

We consider that in equations (9.28) coordinates $x_1^{(o)}, y_1^{(o)}$ and $z_1^{(o)}$ for the reference point are known and the equation system must be solved for three unknowns. Taking $y_m^{(o)} = 0$, we may represent the solution for the unknowns $x_m^{(o)}, z_m^{(o)}$ and δ as follows

$$x_m^{(o)} = [(y_1^{(o)})^2 + (z_1^{(o)})^2]^{\frac{1}{2}} \tag{9.29}$$

$$\tan\frac{\delta}{2} = -\frac{(y_1^{(o)})^2 + (z_1^{(o)})^2 + z_1^{(o)}x_m^{(o)}}{y_1^{(o)}x_m^{(o)}} \tag{9.30}$$

$$z_m^{(o)} = -x_1^{(o)} \tag{9.31}$$

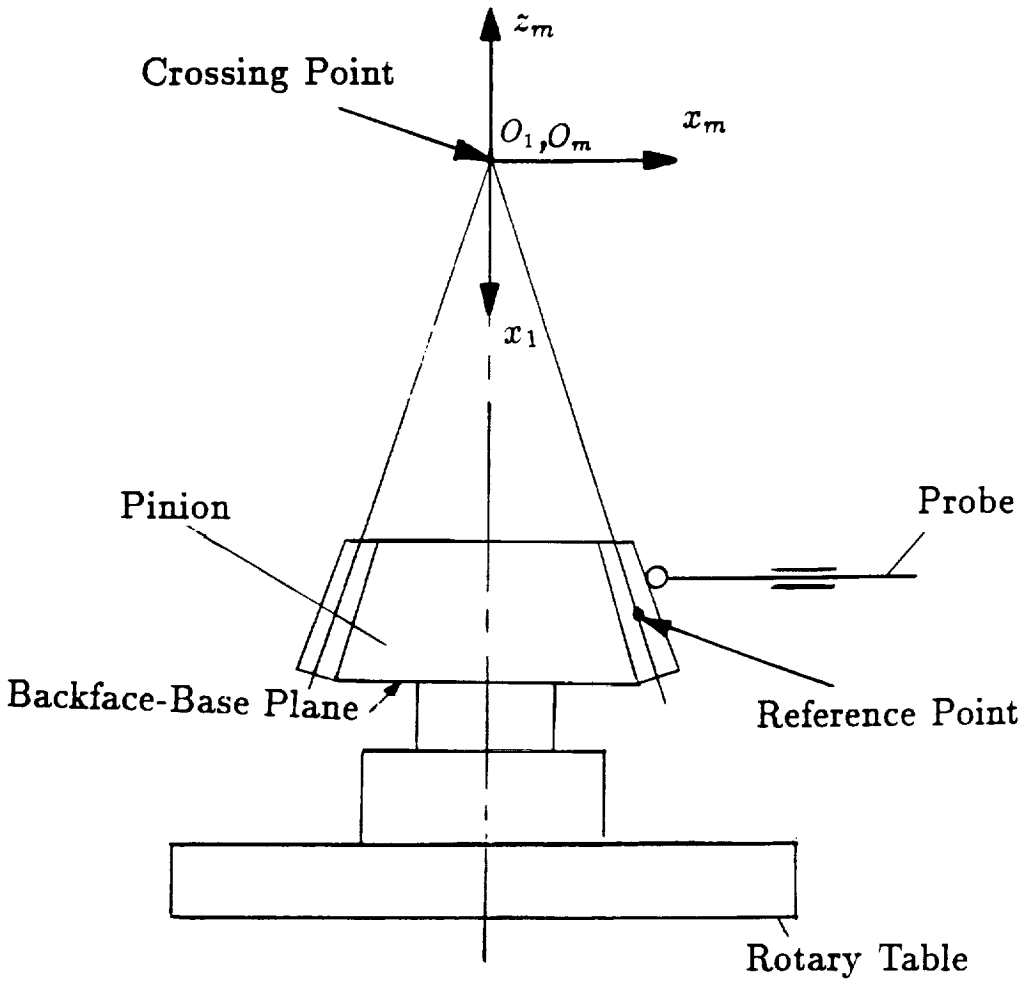

Figure 9.6: Pinion Measurement

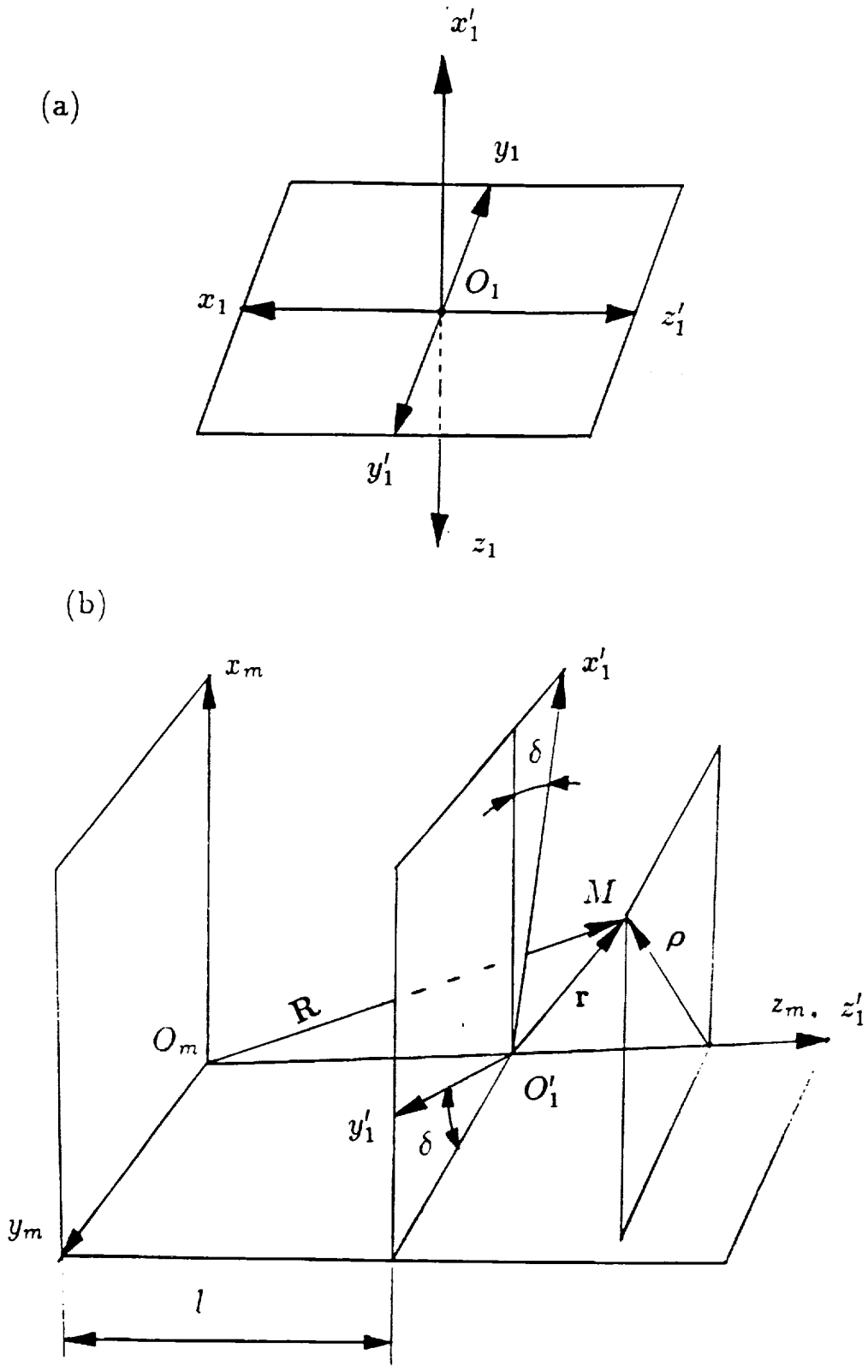

Figure 9.7: Coordinate Transformation

After obtaining the angle of δ, the theoretical pinion tooth surface Σ_1 can be represented in S_m by using equation (9.26). Similarly, the unit normal to the theoretical pinion tooth surface can be represented in S_m as

$$[n_m] = [L_{m1}][n_1] \tag{9.32}$$

where,

$$[L_{m1}] = \begin{bmatrix} 0 & -\sin\delta & -\cos\delta \\ 0 & -\cos\delta & \sin\delta \\ -1 & 0 & 0 \end{bmatrix} \tag{9.33}$$

The coordinates of probe center $\boldsymbol{\rho}_m^{(o)} = [X_m^{(o)}, Y_m^{(o)}, Z_m^{(o)}]^T$ on surface $\Sigma_{(c)m}$ that correspond to reference point $(x_1^{(o)}, y_1^{(o)}, z_1^{(o)})$ on theoretical surface Σ_1 can be determined in S_m with equation similar to (9.25). For the initial installment the pinion tooth surface must be brought into contact with the probe while the probe center is at $(X_m^{(o)}, Y_m^{(o)}, Z_m^{(o)})$. Then, the pinion tooth surface is fixed in the rest of measurement process, while the probe performs the translational motions.

Based on the above considerations, the procedure of initial installment can be obtained as follows:

(i) Install the probe with coordinates $(X_m^{(0)}, Y_m^{(0)}, Z_m^{(0)})$ that are represented as follows:

$$\left.\begin{array}{rcl} X_m^{(0)} & = & x_m^{(0)} + an_{xm}^{(0)} \\ Y_m^{(0)} & = & y_m^{(0)} + an_{ym}^{(0)} \\ Z_m^{(0)} & = & z_m^{(0)} + an_{zm}^{(0)} \end{array}\right\} \tag{9.34}$$

Here: $n_{xm}^{(0)}$, $n_{ym}^{(0)}$ and $n_{zm}^{(0)}$ are the components of the theoretical surface normal at the reference point; a is the radius of the ball surface of the probe.

(ii) Turn the rotary table until the probe contacts the to-be-measured surface. The value of δ for this installation is given by equation (9.30).

9.5 Determination of Deviations of Real Tooth Surface

We consider in coordinate system S_m two surfaces: (i) $\Sigma_{(e)m}$ that might be traced out in S_m by the center of the probe if the pinion tooth surface is an ideal surface, and (ii) surface $\Sigma^{\star}_{(e)m}$ that is traced out in reality by the center of the probe in the case when the pinion tooth surface is a real surface.

The position vector of the probe center for the theoretical equidistant surface $\Sigma_{(e)m}$ is determined in S_m with the equation similar to (9.25), i.e.,

$$\boldsymbol{\rho}_{mi} = \mathbf{r}_{mi}(\phi_{1i}, \theta_{Fi}, d_j) + a\mathbf{n}_{mi}(\phi_{1i}, \theta_{Fi}, d_k) \qquad (i = 1, \ldots, 45) \tag{9.35}$$

By measurements of the real surface the position vector of the probe center may be represented as

$$\mathbf{R}_{mi} = \mathbf{r}_{mi}(\phi_{1i}, \theta_{Fi}, d_j) + \lambda_i \mathbf{n}_{mi}(\phi_{1i}, \theta_{Fi}, d_k) \qquad (i = 1, \ldots, 45) \tag{9.36}$$

where λ_i determines the real location of the probe center on surface $\Sigma^{\star}_{(e)}$ and is considered along the normal to the theoretical surface.

Subscript "m" indicates that both surfaces are represented in S_m; subscript "i" indicates the current point of the grid; (ϕ_{1i} and θ_{Fi}) are Gaussian coordinates of the theoretical tooth surface Σ that are known for each grid point; d_j ($j = 1, \ldots, 8$) represent the linear and angular machine tool settings designated by $E_m, \triangle B, \triangle A, S_R, \theta_c, j, i, \gamma_m$ (Fig. 9.1, 9.2, 9.3); d_k ($k = 1, \ldots, 4$) represent the angular machine-tool settings designated by θ_c, j, i, γ_m.

Equations (9.35) and (9.36) yield

$$a = (\rho_{mi} - \mathbf{r}_{mi}) \cdot \mathbf{n}_{mi} \tag{9.37}$$

$$\lambda_i = (\mathbf{R}_{mi} - \mathbf{r}_{mi}) \cdot \mathbf{n}_{mi} \tag{9.38}$$

The deviation of the real tooth surface Σ^* from the theoretical surface Σ is measured along the normal to the theoretical surface and can be represented as

$$\triangle b_i = \lambda_i - a = (\mathbf{R}_{mi} - \rho_{mi}) \cdot \mathbf{n}_{mi} \tag{9.39}$$

Taking into account equations (9.39) and (9.38) we obtain that

$$\triangle b_i = \lambda_i - a = (X^*_{mi} - X_{mi}) \cdot n_{xmi} + (Y^*_{mi} - Y_{mi}) \cdot n_{ymi} + (Z^*_{mi} - Z_{mi}) \cdot n_{zmi} \tag{9.40}$$

where $(X^*_{mi}, Y^*_{mi}, Z^*_{mi})$ are the coordinates of the center of the probe obtained by measurements; (X_{mi}, Y_{mi}, Z_{mi}) are the coordinates of the center of the probe for surface $\Sigma_{(e)m}$ that is equidistant to the theoretical surface Σ_m.

9.6 Mathematical Aspects of Minimization

We consider two steps for computerized minimization of deviations of real tooth surfaces:

(1). development of relations between corrections of machine-tool settings and surface deviations;

(2). minimization of deviations (see chapter 7).

Step 1.: Variation of Tooth Surface Caused by Change of Machine-Tool Settings

The pinion tooth surface in accordance to expressions (9.21) and (9.22) is represented in S_m as follows

$$\mathbf{r}_m = \mathbf{r}_{mi}(\phi_{1i}, \theta_{Fi}, d_j) \;\; ; \;\; \mathbf{n}_m = \mathbf{n}_m(\phi_{1i}, \theta_{Fi}, d_k) \tag{9.41}$$

For simplicity, the subscript "m" is dropped in the following derivations. The first order variations of the surface that is caused by the change of machine-tool settings and surface coordinates is represented as

$$\triangle \mathbf{r}_i = \frac{\partial \mathbf{r}}{\partial \theta_F} \triangle \vartheta_F + \frac{\partial \mathbf{r}}{\partial \phi_1} \triangle \phi_1 + \sum_{j=1}^{8} \frac{\partial \mathbf{r}_i}{\partial d_j} \triangle d_j \tag{9.42}$$

The normal deviation of the surface at grid point i can be represented by

$$\triangle r_{ni} = \triangle \mathbf{r}_i \cdot (\mathbf{n}_i^*) \tag{9.43}$$

where $\mathbf{n}_i^* = \frac{\mathbf{n}+\triangle \mathbf{n}}{|\mathbf{n}+\triangle \mathbf{n}|}$

Here: $\triangle \mathbf{n}_i$ is the variation of surface unit normal ; $|\mathbf{n}_i^*| = 1$.

Since we consider the first order deviations, we can represent the deviations $\triangle r_{ni}$ by

$$\triangle r_{ni} = \triangle \mathbf{r}_i \cdot \mathbf{n}_i = \sum_{j=1}^{8} (\frac{\partial \mathbf{r}_i}{\partial d_j} \triangle d_j) \cdot \mathbf{n}_i \tag{9.44}$$

While deriving equation (9.44) we have taken into account that $\frac{\partial \mathbf{r}}{\partial \theta_F} \cdot \mathbf{n} = \frac{\partial \mathbf{r}}{\partial \phi_1} \cdot \mathbf{n} = 0$ because vectors $\frac{\partial \mathbf{r}}{\partial \theta_F}$ and $\frac{\partial \mathbf{r}}{\partial \phi_1}$ lie in the plane that is tangent to the surface.

Step 2.: Linear Equations

The surface normal variations must be equal to the deviations obtained by measurements. Thus we will obtain an overdetermined system of n linear equations in eight unknowns represented as

$$\sum_{j=1}^{8} (\frac{\partial \mathbf{r}_i}{\partial d_j} \triangle d_j) \cdot \mathbf{n}_i = \triangle b_i \tag{9.45}$$

The number of equations, n, is equal to the number of measurements (the number of grid points). In this example, 8 machine-tool settings are considered. The mathematical aspect of the problem is the determination of such eight unknowns of $\triangle d_j$ that will minimize the difference of the right and left sides of equation system (9.45). One of the widely used methods for the solution of the overdetermined system of linear equations is the least-square method. In this work we have used the subroutine DLSQRR of IMSL MATH/LIBRARY [7] for the numerical solution.

9.3 Results of Coordinate Measurements and Minimization of Deviations for hypoid pinions

The numerical example is based on the experiment that has been performed at the Dana Corporation (Fort Wayne, USA). The deviations of real pinion tooth surfaces for both sides of the pinion tooth have been obtained by measurements on the Zeiss machine. The developed approach has been used for minimization of obtained deviations. Fig. 9.8 and Fig. 9.9 illustrate the deviations $\triangle b_i$ of the real surface from the theoretical one, that have been obtained by measurements and calculations for the concave side and convex side, respectively. Based on the corrected machine-

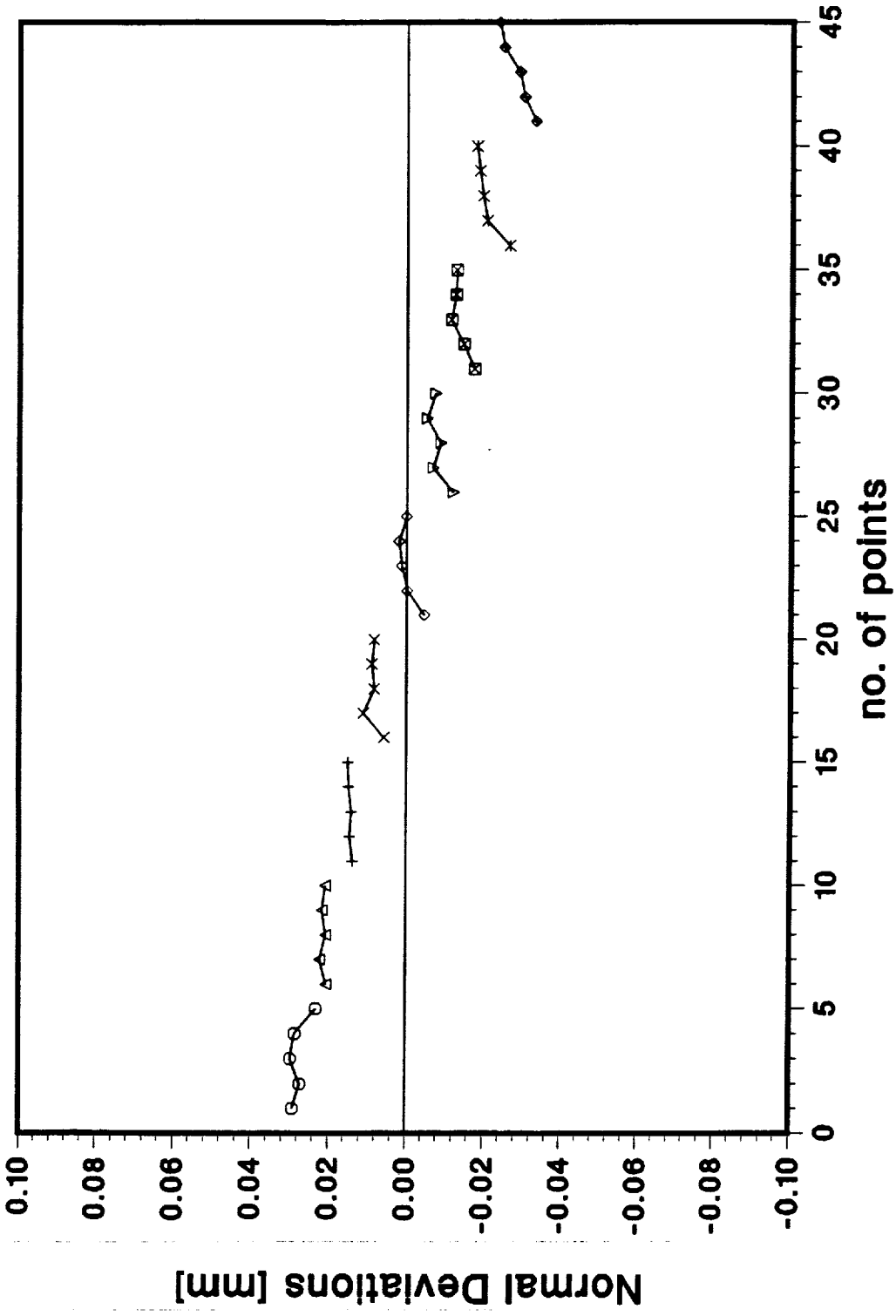

Figure 9.8: Deviations of Pinion Real Tooth Surface (Concave Side)

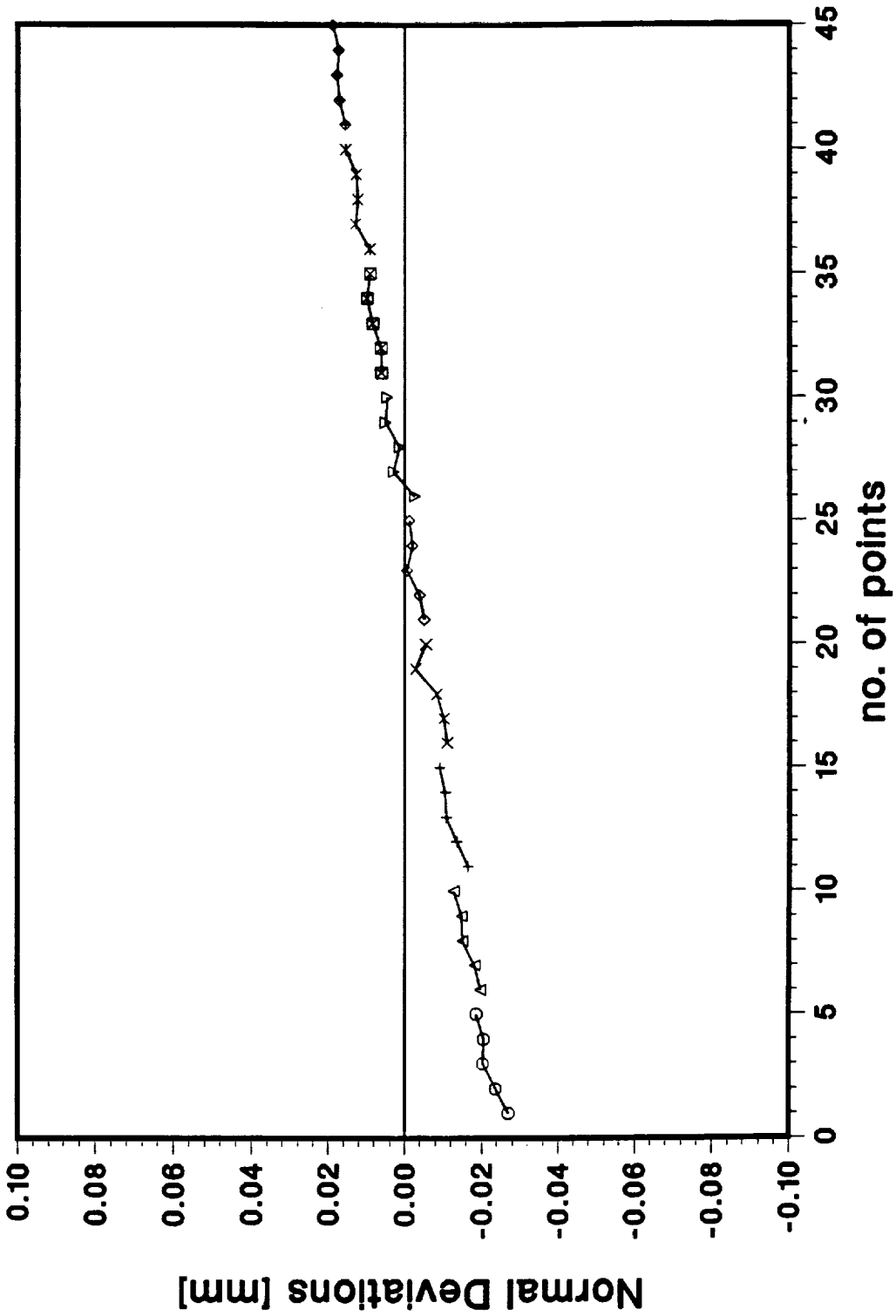

Figure 9.9: Deviations of Pinion Real Tooth Surface (Convex Side)

tool settings, we can manufacture a new surface that will optimally fit the theoretical surface after the surface is distorted by heat-treatment and manufacturing process, etc. The results of performed experiment for minimized deviations between the new surface and the theoretical surface are very favorable, that is illustrated with drawings in Fig. 9.10 and Fig. 9.11 for concave side and convex side, respectively.

Experimental Data

The experimental data are represented in tables in Appendix (Table B.1-B.7 for concave side, Table C.1-C.7 for convex side)

(1) Blank data of hypoid pinion

(2) Initial basic machine-tool settings

(3) Coordinates of theoretical surface Σ

(4) Projections of surface unit normal

(5) Coordinates of real surface Σ^* (obtained by measurements)

(6) Corrected machine-tool settings

(7) Corrections of machine-tool settings

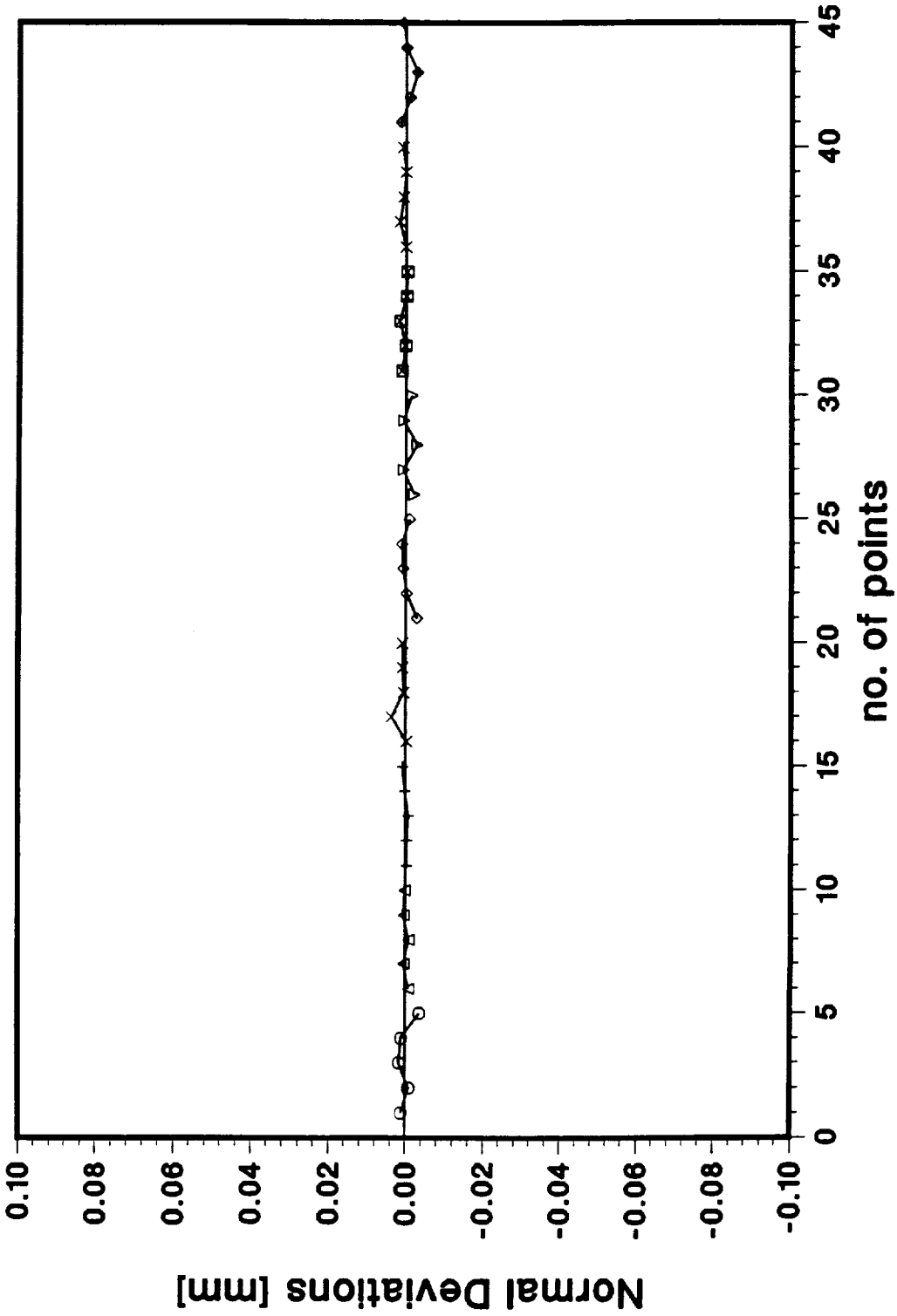

Figure 9.10: Minimized Deviations (Concave Side)

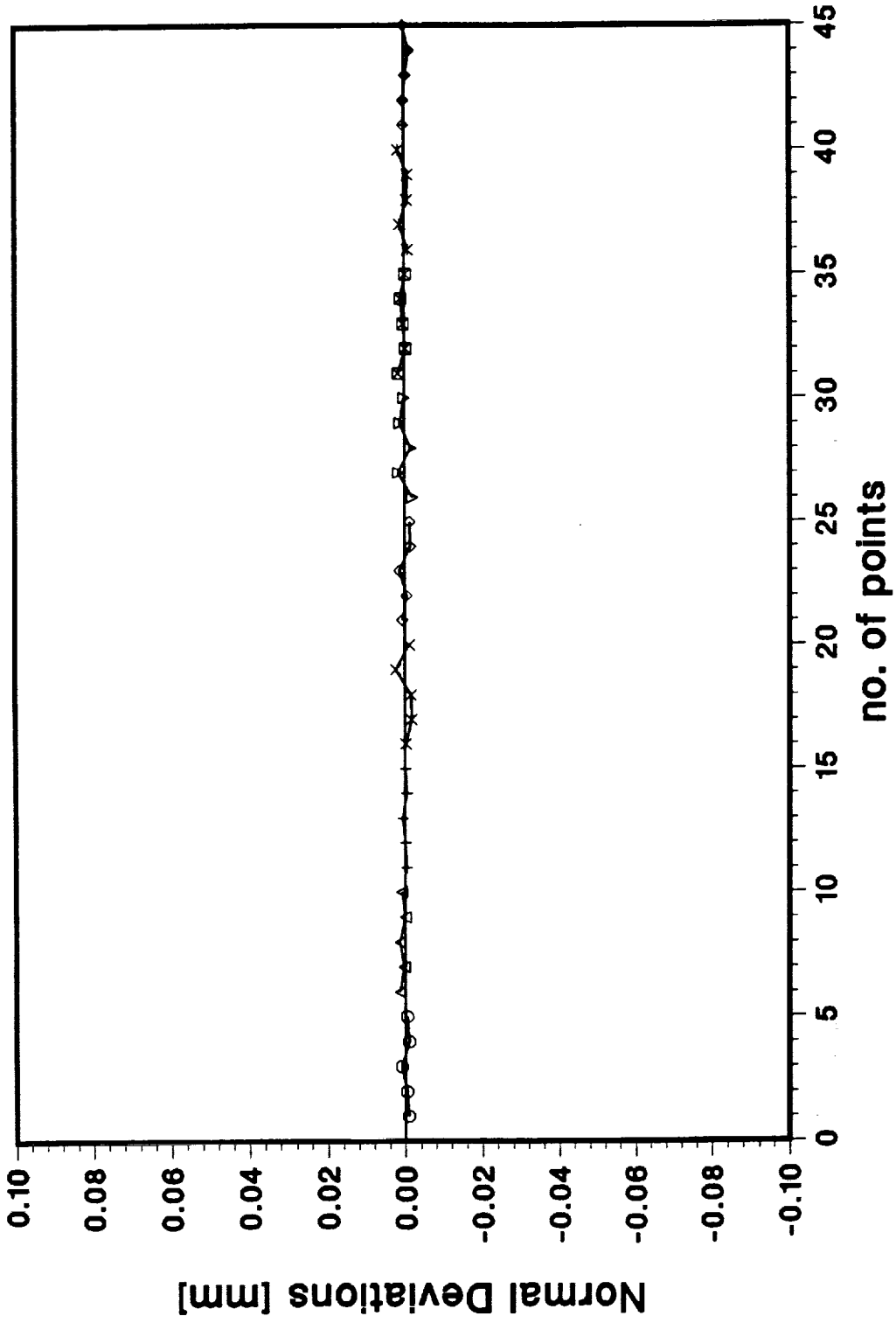

Figure 9.11: Minimized Deviations (Convex Side)

Appendix A

Table A.1: *RESULTS OF MINIMIZATION FOR DANA HYPOID GEAR*

INPUT DATA :	
Pressure Angle α_G	$21.25°$
Cutter diameter	$228.6mm$
Point Width of Cutter	$2.032mm$

BASIC MACHINE-TOOL SETTINGS :	
V_2(Vertical Setting)	$103.25255mm$
H_2(Horizontal Setting)	$27.4666mm$
$\gamma_m^{(2)}$(Machine Root Angle)	$60.723°$
$\triangle X_m$(Machine Center to Back)	$0.009677mm$

CORRECTIONS OF MACHINE-TOOL SETTINGS REQUIRED :	
V_2(Vertical Setting)	$-0.000361mm$
H_2(Horizontal Setting)	$-0.250553mm$
$\gamma_m^{(2)}$(Machine Root Angle)	$0.260867°$
$\triangle X_m$(Machine Center To Back)	$-0.543113mm$

CORRECTED MACHINE-TOOL SETTINGS:	
V_2(Vertical Setting)	$103.2522mm$
H_2(Horizontal Setting)	$27.21603mm$
$\gamma_m^{(2)}$(Machine Root Angle)	$60.98391°$
$\triangle X_m$(Machine Center to Back)	$-0.53343mm$

****

Table A.2 Coordinates of Theoretical Surface (Convex Side)
(represented in Sm (Fig. 3.2))

****

		XT (inch)	YT (inch)	ZT (inch)
1	1	3.128970	0.2903200	-1.660430
1	2	3.149190	0.2766600	-1.612140
1	3	3.169320	0.2630300	-1.563840
1	4	3.189390	0.2494500	-1.515550
1	5	3.209370	0.2358900	-1.467260
2	1	3.247090	0.2322700	-1.715660
2	2	3.267980	0.2179600	-1.664110
2	3	3.288790	0.2036900	-1.612550
2	4	3.309520	0.1894600	-1.561000
2	5	3.330190	0.1752700	-1.509450
3	1	3.364070	0.1699200	-1.770890
3	2	3.385620	0.1549900	-1.716080
3	3	3.407080	0.1401000	-1.661260
3	4	3.428470	0.1252500	-1.606450
3	5	3.449790	0.1104400	-1.551640
4	1	3.479810	0.1032600	-1.826120
4	2	3.501990	0.8771000E-01	-1.768050
4	3	3.524090	0.7221000E-01	-1.709970
4	4	3.546120	0.5676000E-01	-1.651900
4	5	3.568090	0.4134000E-01	-1.593830
5	1	3.594170	0.3223000E-01	-1.881350
5	2	3.616970	0.1609000E-01	-1.820020
5	3	3.639700	0.0000000E+00	-1.758680
5	4	3.662360	-0.1605000E-01	-1.697350
5	5	3.684950	-0.3206000E-01	-1.636020
6	1	3.707040	-0.4318000E-01	-1.936580
6	2	3.730450	-0.5990000E-01	-1.871980
6	3	3.753790	-0.7658000E-01	-1.807390
6	4	3.777060	-0.9322000E-01	-1.742800
6	5	3.800270	-0.1098100	-1.678210
7	1	3.818290	-0.1230000	-1.991800
7	2	3.842300	-0.1403100	-1.923950
7	3	3.866230	-0.1575700	-1.856100
7	4	3.890110	-0.1747800	-1.788260
7	5	3.913920	-0.1919500	-1.720410
8	1	3.927780	-0.2072700	-2.047030

8	2	3.952370	-0.2251500	-1.975920
8	3	3.976900	-0.2429900	-1.904810
8	4	4.001360	-0.2607900	-1.833710
8	5	4.025760	-0.2785400	-1.762600
9	1	4.035380	-0.2960100	-2.102260
9	2	4.060540	-0.3144800	-2.027890
9	3	4.085640	-0.3329100	-1.953520
9	4	4.110680	-0.3512900	-1.879160
9	5	4.135660	-0.3696300	-1.804790

****

Table A.3 Coordinates of Theoretical Surface (Concave Side)
(represented in Sm (Fig. 3.2))

****

		XT (inch)	YT (inch)	ZT (inch)
10	1	3.133200	0.1974800	-1.666550
10	2	3.150790	0.2285300	-1.616730
10	3	3.168110	0.2595400	-1.566910
10	4	3.185160	0.2904800	-1.517080
10	5	3.201940	0.3213800	-1.467260
11	1	3.249620	0.1343800	-1.721780
11	2	3.268670	0.1681800	-1.668700
11	3	3.287400	0.2019200	-1.615620
11	4	3.305810	0.2356100	-1.562530
11	5	3.323910	0.2692400	-1.509450
12	1	3.364720	0.6628000E-01	-1.777010
12	2	3.385350	0.1029300	-1.720670
12	3	3.405610	0.1395300	-1.664330
12	4	3.425490	0.1760700	-1.607980
12	5	3.445010	0.2125400	-1.551640
13	1	3.478340	-0.6930000E-02	-1.832240
13	2	3.500690	0.3269000E-01	-1.772640
13	3	3.522590	0.7226000E-01	-1.713040
13	4	3.544070	0.1117600	-1.653440
13	5	3.565120	0.1511900	-1.593830
14	1	3.590310	-0.8535000E-01	-1.887470
14	2	3.614510	-0.4265000E-01	-1.824610
14	3	3.638210	0.0000000E+00	-1.761750
14	4	3.661400	0.4258000E-01	-1.698890
14	5	3.684110	0.8508000E-01	-1.636020
15	1	3.700440	-0.1691000	-1.942700
15	2	3.726650	-0.1232100	-1.876580
15	3	3.752280	-0.7736000E-01	-1.810460
15	4	3.777330	-0.3159000E-01	-1.744340
15	5	3.801830	0.1411000E-01	-1.678210
16	1	3.808520	-0.2583200	-1.997930
16	2	3.836920	-0.2091100	-1.928550
16	3	3.864640	-0.1599500	-1.859170
16	4	3.891700	-0.1108600	-1.789790
16	5	3.918130	-0.6185000E-01	-1.720410
17	1	3.914360	-0.3531200	-2.053160

17	2	3.945110	-0.3004800	-1.980520
17	3	3.975100	-0.2478900	-1.907880
17	4	4.004340	-0.1953600	-1.835240
17	5	4.032850	-0.1429100	-1.762600
18	1	4.017700	-0.4536600	-2.108390
18	2	4.051000	-0.3974800	-2.032490
18	3	4.083450	-0.3413300	-1.956590
18	4	4.115050	-0.2852300	-1.880690
18	5	4.145820	-0.2292100	-1.804790

****

Table A.4 Projections of Surface Unit Normal (Convex Side)
(represented in Sm (Fig. 3.2))

****

		XN (inch)	YN (inch)	ZN (inch)
1	1	0.4496000	0.8910000	0.6380000E-01
1	2	0.4500000	0.8908000	0.6360000E-01
1	3	0.4504000	0.8906000	0.6350000E-01
1	4	0.4508000	0.8904000	0.6330000E-01
1	5	0.4512000	0.8902000	0.6310000E-01
2	1	0.4743000	0.8789000	0.5180000E-01
2	2	0.4747000	0.8786000	0.5150000E-01
2	3	0.4751000	0.8784000	0.5130000E-01
2	4	0.4755000	0.8782000	0.5110000E-01
2	5	0.4759000	0.8780000	0.5090000E-01
3	1	0.4988000	0.8658000	0.3990000E-01
3	2	0.4992000	0.8656000	0.3960000E-01
3	3	0.4997000	0.8653000	0.3940000E-01
3	4	0.5001000	0.8651000	0.3920000E-01
3	5	0.5006000	0.8648000	0.3900000E-01
4	1	0.5231000	0.8518000	0.2820000E-01
4	2	0.5236000	0.8515000	0.2790000E-01
4	3	0.5241000	0.8512000	0.2770000E-01
4	4	0.5246000	0.8509000	0.2750000E-01
4	5	0.5251000	0.8506000	0.2720000E-01
5	1	0.5472000	0.8368000	0.1670000E-01
5	2	0.5478000	0.8365000	0.1650000E-01
5	3	0.5483000	0.8361000	0.1620000E-01
5	4	0.5489000	0.8358000	0.1600000E-01
5	5	0.5494000	0.8354000	0.1570000E-01
6	1	0.5711000	0.8208000	0.5500000E-02
6	2	0.5717000	0.8204000	0.5200000E-02
6	3	0.5723000	0.8200000	0.5000000E-02
6	4	0.5729000	0.8196000	0.4700000E-02
6	5	0.5735000	0.8192000	0.4400000E-02
7	1	0.5947000	0.8039000	-0.5400000E-02
7	2	0.5954000	0.8034000	-0.5700000E-02
7	3	0.5961000	0.8029000	-0.6000000E-02
7	4	0.5967000	0.8024000	-0.6300000E-02
7	5	0.5974000	0.8019000	-0.6700000E-02
8	1	0.6180000	0.7860000	-0.1610000E-01

8	2	0.6188000	0.7854000	-0.1640000E-01
8	3	0.6195000	0.7848000	-0.1680000E-01
8	4	0.6203000	0.7842000	-0.1710000E-01
8	5	0.6210000	0.7836000	-0.1740000E-01
9	1	0.6410000	0.7671000	-0.2640000E-01
9	2	0.6419000	0.7664000	-0.2680000E-01
9	3	0.6427000	0.7656000	-0.2720000E-01
9	4	0.6435000	0.7649000	-0.2760000E-01
9	5	0.6444000	0.7642000	-0.2790000E-01

****

Table A.5 Projections of Surface Unit Normal (Concave Side)
(represented in Sm (Fig. 3.2))

****

		XN (inch)	YN (inch)	ZN (inch)
10	1	-0.1557000	-0.8123000	0.5620000
10	2	-0.1524000	-0.8141000	0.5604000
10	3	-0.1492000	-0.8159000	0.5587000
10	4	-0.1459000	-0.8176000	0.5570000
10	5	-0.1426000	-0.8193000	0.5553000
11	1	-0.1789000	-0.7991000	0.5740000
11	2	-0.1753000	-0.8012000	0.5721000
11	3	-0.1718000	-0.8033000	0.5703000
11	4	-0.1682000	-0.8053000	0.5685000
11	5	-0.1646000	-0.8073000	0.5667000
12	1	-0.2019000	-0.7850000	0.5857000
12	2	-0.1981000	-0.7874000	0.5838000
12	3	-0.1943000	-0.7898000	0.5818000
12	4	-0.1904000	-0.7922000	0.5799000
12	5	-0.1865000	-0.7945000	0.5779000
13	1	-0.2248000	-0.7699000	0.5973000
13	2	-0.2207000	-0.7727000	0.5952000
13	3	-0.2166000	-0.7754000	0.5931000
13	4	-0.2124000	-0.7782000	0.5911000
13	5	-0.2083000	-0.7809000	0.5889000
14	1	-0.2475000	-0.7538000	0.6087000
14	2	-0.2431000	-0.7570000	0.6065000
14	3	-0.2387000	-0.7602000	0.6043000
14	4	-0.2343000	-0.7633000	0.6021000
14	5	-0.2298000	-0.7664000	0.5999000
15	1	-0.2699000	-0.7367000	0.6200000
15	2	-0.2653000	-0.7404000	0.6176000
15	3	-0.2606000	-0.7440000	0.6153000
15	4	-0.2559000	-0.7475000	0.6130000
15	5	-0.2512000	-0.7510000	0.6106000
16	1	-0.2922000	-0.7187000	0.6310000
16	2	-0.2872000	-0.7228000	0.6285000
16	3	-0.2823000	-0.7268000	0.6261000
16	4	-0.2773000	-0.7309000	0.6236000
16	5	-0.2724000	-0.7348000	0.6216000
17	1	-0.3141000	-0.6996000	0.6418000

17	2	-0.3090000	-0.7042000	0.6393000
17	3	-0.3038000	-0.7088000	0.6367000
17	4	-0.2986000	-0.7133000	0.6341000
17	5	-0.2933000	-0.7177000	0.6315000
18	1	-0.3359000	-0.6794000	0.6524000
18	2	-0.3304000	-0.6846000	0.6497000
18	3	-0.3250000	-0.6897000	0.6471000
18	4	-0.3195000	-0.6947000	0.6444000
18	5	-0.3140000	-0.6997000	0.6417000

C-2

****

Table A.6 Coordinates of Real Tooth Surface (Convex Side)
(represented in Sm (Fig. 3.2))

****

		XM (inch)	YM (inch)	ZM (inch)
1	1	3.129490	0.2913500	-1.660350
1	2	3.149700	0.2776800	-1.612060
1	3	3.169750	0.2638600	-1.563780
1	4	3.189690	0.2500400	-1.515510
1	5	3.209520	0.2361800	-1.467240
2	1	3.247520	0.2330600	-1.715610
2	2	3.268290	0.2185300	-1.664070
2	3	3.289010	0.2041000	-1.612530
2	4	3.309610	0.1896300	-1.560990
2	5	3.330130	0.1751800	-1.509460
3	1	3.364450	0.1705700	-1.770860
3	2	3.385850	0.1553900	-1.716060
3	3	3.407190	0.1402900	-1.661260
3	4	3.428470	0.1252400	-1.606450
3	5	3.449590	0.1101000	-1.551660
4	1	3.480060	0.1036700	-1.826100
4	2	3.502140	0.8796000E-01	-1.768040
4	3	3.524200	0.7239000E-01	-1.709970
4	4	3.546040	0.5661000E-01	-1.651910
4	5	3.567790	0.4086000E-01	-1.593850
5	1	3.594330	0.3248000E-01	-1.881340
5	2	3.617010	0.1615000E-01	-1.820010
5	3	3.639690	-0.2000000E-04	-1.758680
5	4	3.662250	-0.1622000E-01	-1.697360
5	5	3.684770	-0.3233000E-01	-1.636030
6	1	3.707180	-0.4297000E-01	-1.936570
6	2	3.730500	-0.5983000E-01	-1.871980
6	3	3.753810	-0.7655000E-01	-1.807390
6	4	3.777040	-0.9324000E-01	-1.742800
6	5	3.800210	-0.1098800	-1.678210
7	1	3.818310	-0.1229700	-1.991800
7	2	3.842330	-0.1402600	-1.923950
7	3	3.866260	-0.1575300	-1.856100
7	4	3.890240	-0.1746000	-1.788260
7	5	3.914230	-0.1915300	-1.720410
8	1	3.927840	-0.2071900	-2.047030

8	2	3.952510	-0.2249800	-1.975930
8	3	3.977000	-0.2428600	-1.904820
8	4	4.001410	-0.2607300	-1.833710
8	5	4.025690	-0.2786400	-1.762590
9	1	4.035370	-0.2960200	-2.102260
9	2	4.060560	-0.3144600	-2.027890
9	3	4.085710	-0.3328300	-1.953530
9	4	4.110690	-0.3512800	-1.879160
9	5	4.135620	-0.3696800	-1.804780

****

Table A.7 Coordinates of Real Tooth Surface (Concave Side)
(represented in Sm (Fig. 3.2))

****

		XM (inch)	YM (inch)	ZM (inch)
10	1	3.132990	0.1964100	-1.665810
10	2	3.150610	0.2275400	-1.616050
10	3	3.167920	0.2585200	-1.566210
10	4	3.184990	0.2895700	-1.516460
10	5	3.201810	0.3206400	-1.466760
11	1	3.249400	0.1334300	-1.721100
11	2	3.268500	0.1673900	-1.668130
11	3	3.287250	0.2012300	-1.615120
11	4	3.305660	0.2349100	-1.562040
11	5	3.323800	0.2687000	-1.509070
12	1	3.364540	0.6559000E-01	-1.776500
12	2	3.385210	0.1023500	-1.720240
12	3	3.405490	0.1390500	-1.663970
12	4	3.425410	0.1757200	-1.607730
12	5	3.444970	0.2123700	-1.551520
13	1	3.478190	-0.7460000E-02	-1.831830
13	2	3.500600	0.3238000E-01	-1.772390
13	3	3.522530	0.7202000E-01	-1.712860
13	4	3.544050	0.1116800	-1.653370
13	5	3.565170	0.1513600	-1.593960
14	1	3.590180	-0.8574000E-01	-1.887160
14	2	3.614450	-0.4283000E-01	-1.824460
14	3	3.638200	-0.1000000E-04	-1.761740
14	4	3.661460	0.4279000E-01	-1.699050
14	5	3.684250	0.8554000E-01	-1.636390
15	1	3.700360	-0.1693200	-1.942510
15	2	3.726640	-0.1232300	-1.876550
15	3	3.752350	-0.7716000E-01	-1.810620
15	4	3.777450	-0.3124000E-01	-1.744620
15	5	3.802060	0.1480000E-01	-1.678780
16	1	3.808470	-0.2584400	-1.997820
16	2	3.836960	-0.2090000	-1.928640
16	3	3.864780	-0.1596000	-1.859460
16	4	3.891920	-0.1102900	-1.790270
16	5	3.918530	-0.6077000E-01	-1.721310
17	1	3.914340	-0.3531600	-2.053120

17	2	3.945230	-0.3002000	-1.980770
17	3	3.975310	-0.2474000	-1.908320
17	4	4.004620	-0.1946900	-1.835830
17	5	4.033320	-0.1417500	-1.763610
18	1	4.017820	-0.4534000	-2.108630
18	2	4.051260	-0.3969500	-2.032980
18	3	4.083780	-0.3406200	-1.957250
18	4	4.115450	-0.2843600	-1.881500
18	5	4.146320	-0.2280800	-1.805820

****
* TABLE B.1. BLANK DATA OF HYPOID PINION *
****

NUMBER OF TEETH: 13
SHAFT ANGLE: 1.57079 radians
PITCH DIAMETER: 88.22 mm
OUTSIDE DIAMETER: 103.96 mm
PITCH ANGLE: 0.32055 radians
FACE ANGLE: 0.41480 radians
ROOT ANGLE: 0.30136 radians
MEAN SPIRAL ANGLE: 0.84677 radians
FACE WIDTH: 38.30 mm
WHOLE WIDTH: 11.63 mm
HAND OF SPIRAL: R.H.

****
TABLE B.2 BASIC PINION MACHINE-TOOL SETTINGS (CONCAVE SIDE)
****

BASIC TILT ANGLE :	CI =	0.4104054	radians
SWIVEL ANGLE :	CJ =	6.000656	radians
MACHINE ROOT ANGLE :	RGMAIM =	6.229372	radians
CRADLE ANGLE :	QC =	1.566173	radians
RADIAL SETTING :	SR =	109.6660	mm
SLIDING BASE :	DELTB =	14.82000	mm
MACHINE CENTER TO BACK:	DELTA =	-3.100000	mm
BLANK OFFSET :	EM =	-34.58000	mm
CUTTING RATIO :	FM1 =	0.3230215	
CUTTER POINT RADIUS :	RCF =	113.0300	mm
CUTTER BLADE ANGLE :	PHIV1C =	0.2443461	radians

****

Table B.3 Coordinates of Theoretical Surface (Concave Side)
(represented in Sm (Fig. 3.2))

****

		XT (inch)	YT (inch)	ZT (inch)
1	1	1.182150	0.5780900	-2.843880
1	2	1.209360	0.6126500	-2.830410
1	3	1.234970	0.6497300	-2.816930
1	4	1.258970	0.6891100	-2.803460
1	5	1.281330	0.7306100	-2.789990
2	1	1.288970	0.4359300	-2.987910
2	2	1.323870	0.4692300	-2.973160
2	3	1.357280	0.5057100	-2.958410
2	4	1.389190	0.5450800	-2.943660
2	5	1.419540	0.5871400	-2.928910
3	1	1.376770	0.2825600	-3.131950
3	2	1.419280	0.3132400	-3.115920
3	3	1.460570	0.3477800	-3.099890
3	4	1.500570	0.3858300	-3.083860
3	5	1.539180	0.4271500	-3.067830
4	1	1.445230	0.1203900	-3.275980
4	2	1.495080	0.1471400	-3.258680
4	3	1.544110	0.1784300	-3.241370
4	4	1.592160	0.2138500	-3.224060
4	5	1.639110	0.2531100	-3.206760
5	1	1.494220	-0.4833000E-01	-3.420020
5	2	1.550950	-0.2678000E-01	-3.401440
5	3	1.607360	0.0000000E+00	-3.382850
5	4	1.663240	0.3151000E-01	-3.364260
5	5	1.718400	0.6741000E-01	-3.345680
6	1	1.523750	-0.2215400	-3.564050
6	2	1.586690	-0.2063300	-3.544190
6	3	1.649960	-0.1852600	-3.524330
6	4	1.713260	-0.1589100	-3.504460
6	5	1.776320	-0.1276300	-3.484600
7	1	1.533930	-0.3972700	-3.708090
7	2	1.602270	-0.3894600	-3.686950
7	3	1.671710	-0.3752200	-3.665810
7	4	1.741850	-0.3551800	-3.644660
7	5	1.812330	-0.3297300	-3.623520
8	1	1.524960	-0.5736900	-3.852120

8	2	1.597730	-0.5742300	-3.829700
8	3	1.672520	-0.5678200	-3.807290
8	4	1.748770	-0.5551500	-3.784870
8	5	1.826030	-0.5366800	-3.762440
9	1	1.497150	-0.7490500	-3.996160
9	2	1.573260	-0.7587500	-3.972460
9	3	1.652420	-0.7610400	-3.948760
9	4	1.733910	-0.7567400	-3.925070
9	5	1.817170	-0.7462900	-3.901370

****

Table B.4 Projections of Surface Unit Normal (Concave Side)
(represented in Sm (Fig. 3.2))

****

		XN (inch)	YN (inch)	ZN (inch)
1	1	0.2974000	-0.5635000	0.7707000
1	2	0.3205000	-0.5308000	0.7846000
1	3	0.3390000	-0.5003000	0.7967000
1	4	0.3540000	-0.4716000	0.8076000
1	5	0.3662000	-0.4445000	0.8175000
2	1	0.2173000	-0.6032000	0.7674000
2	2	0.2467000	-0.5716000	0.7826000
2	3	0.2704000	-0.5419000	0.7958000
2	4	0.2899000	-0.5138000	0.8074000
2	5	0.3061000	-0.4871000	0.8180000
3	1	0.1340000	-0.6303000	0.7647000
3	2	0.1696000	-0.6008000	0.7812000
3	3	0.1984000	-0.5728000	0.7953000
3	4	0.2223000	-0.5460000	0.8077000
3	5	0.2424000	-0.5203000	0.8189000
4	1	0.4920000E-01	-0.6450000	0.7626000
4	2	0.9090000E-01	-0.6187000	0.7804000
4	3	0.1246000	-0.5932000	0.7954000
4	4	0.1527000	-0.5684000	0.8085000
4	5	0.1764000	-0.5443000	0.8202000
5	1	-0.3530000E-01	-0.6479000	0.7609000
5	2	0.1210000E-01	-0.6257000	0.7800000
5	3	0.5030000E-01	-0.6033000	0.7959000
5	4	0.8220000E-01	-0.5811000	0.8096000
5	5	0.1093000	-0.5592000	0.8218000
6	1	-0.1182000	-0.6395000	0.7597000
6	2	-0.6550000E-01	-0.6222000	0.7801000
6	3	-0.2320000E-01	-0.6038000	0.7968000
6	4	0.1210000E-01	-0.5847000	0.8112000
6	5	0.4220000E-01	-0.5653000	0.8238000
7	1	-0.1983000	-0.6203000	0.7589000
7	2	-0.1408000	-0.6090000	0.7806000
7	3	-0.9480000E-01	-0.5949000	0.7982000
7	4	-0.5650000E-01	-0.5794000	0.8131000
7	5	-0.2380000E-01	-0.5630000	0.8261000
8	1	-0.2742000	-0.5913000	0.7584000

8	2	-0.2126000	-0.5865000	0.7815000
8	3	-0.1637000	-0.5774000	0.7999000
8	4	-0.1228000	-0.5659000	0.8153000
8	5	-0.8790000E-01	-0.5528000	0.8287000
9	1	-0.3452000	-0.5531000	0.7582000
9	2	-0.2800000	-0.5557000	0.7828000
9	3	-0.2287000	-0.5520000	0.8019000
9	4	-0.1859000	-0.5447000	0.8178000
9	5	-0.1492000	-0.5352000	0.8315000

****

Table B.5 Coordinates of Real Tooth Surface (Concave Side)
(represented in Sm (Fig. 3.2))

****

		XM (inch)	YM (inch)	ZM (inch)
1	1	1.182490	0.5774400	-2.843000
1	2	1.209710	0.6120800	-2.829570
1	3	1.235370	0.6491400	-2.816000
1	4	1.259370	0.6885800	-2.802550
1	5	1.281660	0.7302100	-2.789240
2	1	1.289150	0.4354400	-2.987290
2	2	1.324080	0.4687300	-2.972470
2	3	1.357500	0.5052700	-2.957760
2	4	1.389440	0.5446400	-2.942970
2	5	1.419790	0.5867400	-2.928240
3	1	1.376840	0.2822200	-3.131530
3	2	1.419380	0.3129000	-3.115470
3	3	1.460680	0.3474600	-3.099450
3	4	1.500700	0.3855100	-3.083390
3	5	1.539330	0.4268400	-3.067350
4	1	1.445240	0.1202400	-3.275810
4	2	1.495120	0.1468700	-3.258340
4	3	1.544150	0.1782300	-3.241110
4	4	1.592220	0.2136500	-3.223780
4	5	1.639160	0.2529300	-3.206490
5	1	1.494220	-0.4821000E-01	-3.420160
5	2	1.550940	-0.2677000E-01	-3.401440
5	3	1.607360	-0.3000000E-04	-3.382810
5	4	1.663250	0.3146000E-01	-3.364200
5	5	1.718400	0.6741000E-01	-3.345680
6	1	1.523800	-0.2212400	-3.564410
6	2	1.586700	-0.2061600	-3.544400
6	3	1.649970	-0.1850500	-3.524610
6	4	1.713260	-0.1587900	-3.504630
6	5	1.776310	-0.1274600	-3.484840
7	1	1.534060	-0.3968400	-3.708610
7	2	1.602350	-0.3891100	-3.687400
7	3	1.671760	-0.3749500	-3.666170
7	4	1.741880	-0.3548900	-3.645060
7	5	1.812340	-0.3294500	-3.623940
8	1	1.525250	-0.5730800	-3.852910

8	2	1.597910	-0.5737500	-3.830330
8	3	1.672650	-0.5673700	-3.807900
8	4	1.748860	-0.5547300	-3.785470
8	5	1.826090	-0.5362900	-3.763030
9	1	1.497600	-0.7483300	-3.997150
9	2	1.573590	-0.7580900	-3.973390
9	3	1.652680	-0.7604100	-3.949680
9	4	1.734090	-0.7562000	-3.925870
9	5	1.817310	-0.7457900	-3.902150

****
* TABLE B.6 CORRECTED MACHINE-TOOL SETTINGS (CONCAVE SIDE) *
****

BASIC TILT ANGLE :	CI =	0.4360375	radians
SWIVEL ANGLE :	CJ =	6.042021	radians
MACHINE ROOT ANGLE :	RGMA1M =	6.202894	radians
CRADLE ANGLE :	QC =	1.573228	radians
RADIAL SETTING :	SR =	110.4463	mm
SLIDING BASE :	DELTB =	14.82000	mm
MACHINE CENTER TO BACK:	DELTA =	-3.970493	mm
BLANK OFFSET :	EM =	-35.45049	mm
CUTTING RATIO :	FM1 =	0.3230215	
CUTTER POINT RADIUS :	RCF =	113.0300	mm
CUTTER BLADE ANGLE :	PHIV1C =	0.2443461	radians

****
* TABLE B.7 CORRECTIONS OF MACHINE-TOOL SETTINGS (CONCAVE SIDE) *
****

BLANK OFFSET:	EM =	-0.8704924	mm
MACHINE CENTER TO BACK:	DELTA =	-0.5540259	mm
SLIDING BASE :	DELTB =	0.0000000E+00	mm
MACHINE ROOT ANGLE :	RGMA1M =	-0.2647799E-01	radians
RADIAL SETTING :	SR =	0.7803197	mm
CRADLE ANGLE :	QC =	0.7054806E-02	radians
SWIVEL ANGLE :	CJ =	0.4136530E-01	radians
TILT ANGLE :	CI =	0.2563208E-01	radians

****
* TABLE C.1. BLANK DATA OF HYPOID PINION *
****

NUMBER OF TEETH: 13
SHAFT ANGLE: 1.57079 radians
PITCH DIAMETER: 88.22 mm
OUTSIDE DIAMETER: 103.96 mm
PITCH ANGLE: 0.32055 radians
FACE ANGLE: 0.41480 radians
ROOT ANGLE: 0.30136 radians
MEAN SPIRAL ANGLE: 0.84677 radians
FACE WIDTH: 38.30 mm
WHOLE WIDTH: 11.63 mm
HAND OF SPIRAL: R.H.

****
TABLE C.2 BASIC PINION MACHINE-TOOL SETTINGS (CONVEX SIDE)
****

BASIC TILT ANGLE :	CI =	0.3761899	radians
SWIVEL ANGLE :	CJ =	5.766247	radians
MACHINE ROOT ANGLE :	RGMA1M =	6.233736	radians
CRADLE ANGLE :	QC =	1.436986	radians
RADIAL SETTING :	SR =	114.0236	mm
SLIDING BASE :	DELTB =	23.87000	mm
MACHINE CENTER TO BACK:	DELTA =	3.280000	mm
BLANK OFFSET :	EM =	-40.12000	mm
CUTTING RATIO :	FM1 =	0.3020446	
CUTTER POINT RADIUS :	RCF =	114.9350	mm
CUTTER BLADE ANGLE :	PHIV1C =	-0.5410521	radians

****

Table C.3 Coordinates of Theoretical Surface (Convex Side)
(represented in Sm (Fig. 3.2))

****

		XT (inch)	YT (inch)	ZT (inch)
1	1	1.135060	0.6650000	-2.844010
1	2	1.185910	0.6562700	-2.830500
1	3	1.238650	0.6422500	-2.817000
1	4	1.292890	0.6229000	-2.803490
1	5	1.348280	0.5981000	-2.789990
2	1	1.247700	0.5418800	-2.988040
2	2	1.302600	0.5245800	-2.973260
2	3	1.358830	0.5009600	-2.958480
2	4	1.415930	0.4709600	-2.943690
2	5	1.473440	0.4345000	-2.928910
3	1	1.345050	0.4062200	-3.132080
3	2	1.402710	0.3794500	-3.116020
3	3	1.460940	0.3453500	-3.099950
3	4	1.519180	0.3039000	-3.083890
3	5	1.576860	0.2550400	-3.067830
4	1	1.426350	0.2598200	-3.276110
4	2	1.485380	0.2228700	-3.258770
4	3	1.543990	0.1776600	-3.241430
4	4	1.601550	0.1242000	-3.224090
4	5	1.657360	0.6251000E-01	-3.206760
5	1	1.490940	0.1043900	-3.420150
5	2	1.549840	0.5674000E-01	-3.401530
5	3	1.607160	0.0000000E+00	-3.382910
5	4	1.662140	-0.6574000E-01	-3.364290
5	5	1.713980	-0.1403800	-3.345680
6	1	1.538250	-0.5840000E-01	-3.564180
6	2	1.595460	-0.1170800	-3.544290
6	3	1.649730	-0.1855400	-3.524390
6	4	1.700200	-0.2635800	-3.504500
6	5	1.745960	-0.3510200	-3.484600
7	1	1.567790	-0.2269300	-3.708220
7	2	1.621680	-0.2967900	-3.687040
7	3	1.671120	-0.3769300	-3.665870
7	4	1.715140	-0.4670500	-3.644700
7	5	1.752700	-0.5668300	-3.623520
8	1	1.579130	-0.3995700	-3.852250

8	2	1.628050	-0.4805600	-3.829800
8	3	1.670840	-0.5721400	-3.807350
8	4	1.706440	-0.6738600	-3.784900
8	5	1.733720	-0.7852500	-3.762440
9	1	1.571890	-0.5747300	-3.996290
9	2	1.614130	-0.6666000	-3.972560
9	3	1.648460	-0.7691300	-3.948830
9	4	1.673700	-0.8817200	-3.925100
9	5	1.688670	-1.003710	-3.901380

****

Table C.4 Projections of Surface Unit Normal (Convex Side)
(represented in Sm (Fig. 3.2))

****

		XN (inch)	YN (inch)	ZN (inch)
1	1	0.2346000	0.8427000	-0.4846000
1	2	0.3030000	0.8339000	-0.4614000
1	3	0.3662000	0.8201000	-0.4397000
1	4	0.4255000	0.8021000	-0.4190000
1	5	0.4816000	0.7803000	-0.3990000
2	1	0.3421000	0.8087000	-0.4785000
2	2	0.4113000	0.7899000	-0.4549000
2	3	0.4747000	0.7664000	-0.4327000
2	4	0.5336000	0.7389000	-0.4114000
2	5	0.5887000	0.7076000	-0.3908000
3	1	0.4408000	0.7622000	-0.4741000
3	2	0.5093000	0.7335000	-0.4502000
3	3	0.5714000	0.7005000	-0.4276000
3	4	0.6283000	0.6636000	-0.4059000
3	5	0.6809000	0.6232000	-0.3848000
4	1	0.5301000	0.7050000	-0.4712000
4	2	0.5964000	0.6666000	-0.4471000
4	3	0.6558000	0.6245000	-0.4243000
4	4	0.7094000	0.5788000	-0.4022000
4	5	0.7580000	0.5297000	-0.3807000
5	1	0.6097000	0.6386000	-0.4695000
5	2	0.6725000	0.5911000	-0.4454000
5	3	0.7278000	0.5403000	-0.4224000
5	4	0.7768000	0.4864000	-0.4001000
5	5	0.8200000	0.4294000	-0.3783000
6	1	0.6792000	0.5646000	-0.4689000
6	2	0.7372000	0.5086000	-0.4448000
6	3	0.7873000	0.4498000	-0.4217000
6	4	0.8305000	0.3884000	-0.3993000
6	5	0.8674000	0.3244000	-0.3774000
7	1	0.7386000	0.4842000	-0.4692000
7	2	0.7906000	0.4203000	-0.4453000
7	3	0.8343000	0.3543000	-0.4223000
7	4	0.8707000	0.2863000	-0.3999000
7	5	0.9003000	0.2163000	-0.3779000
8	1	0.7874000	0.3985000	-0.4703000

8	2	0.8325000	0.3276000	-0.4467000
8	3	0.8690000	0.2554000	-0.4239000
8	4	0.8976000	0.1817000	-0.4015000
8	5	0.9190000	0.1067000	-0.3795000
9	1	0.8258000	0.3086000	-0.4721000
9	2	0.8630000	0.2317000	-0.4489000
9	3	0.8913000	0.1542000	-0.4264000
9	4	0.9115000	0.7600000E-01	-0.4042000
9	5	0.9240000	-0.2900000E-02	-0.3823000

****

Table C.5 Coordinates of Real Tooth Surface (Convex Side)
(represented in Sm (Fig. 3.2))

****

		XM (inch)	YM (inch)	ZM (inch)
1	1	1.134810	0.6641100	-2.843490
1	2	1.185630	0.6554900	-2.830070
1	3	1.238350	0.6416000	-2.816650
1	4	1.292550	0.6222500	-2.803160
1	5	1.347930	0.5975300	-2.789700
2	1	1.247430	0.5412600	-2.987670
2	2	1.302300	0.5240200	-2.972940
2	3	1.358550	0.5005100	-2.958230
2	4	1.415620	0.4705300	-2.943460
2	5	1.473150	0.4341400	-2.928720
3	1	1.344770	0.4057300	-3.131770
3	2	1.402440	0.3790600	-3.115780
3	3	1.460690	0.3450500	-3.099770
3	4	1.518920	0.3036200	-3.083730
3	5	1.576620	0.2548100	-3.067690
4	1	1.426120	0.2595100	-3.275900
4	2	1.485140	0.2226000	-3.258590
4	3	1.543780	0.1774500	-3.241290
4	4	1.601460	0.1241300	-3.224050
4	5	1.657190	0.6240000E-01	-3.206670
5	1	1.490820	0.1042600	-3.420050
5	2	1.549730	0.5665000E-01	-3.401460
5	3	1.607140	-0.1000000E-04	-3.382900
5	4	1.662070	-0.6578000E-01	-3.364260
5	5	1.713940	-0.1404000	-3.345660
6	1	1.538180	-0.5846000E-01	-3.564130
6	2	1.595550	-0.1170200	-3.544340
6	3	1.649770	-0.1855100	-3.524410
6	4	1.700370	-0.2635000	-3.504580
6	5	1.746120	-0.3509600	-3.484670
7	1	1.567970	-0.2268100	-3.708330
7	2	1.621870	-0.2966800	-3.687150
7	3	1.671390	-0.3768100	-3.666010
7	4	1.715480	-0.4669400	-3.644850
7	5	1.753020	-0.5667500	-3.623650
8	1	1.579410	-0.3994300	-3.852420

8	2	1.628470	-0.4803900	-3.830030
8	3	1.671260	-0.5720100	-3.807550
8	4	1.706890	-0.6737700	-3.785100
8	5	1.734280	-0.7851800	-3.762670
9	1	1.572400	-0.5745400	-3.996570
9	2	1.614710	-0.6664400	-3.972860
9	3	1.649080	-0.7690200	-3.949120
9	4	1.674320	-0.8816700	-3.925370
9	5	1.689350	-1.003710	-3.901660

****
* TABLE C.6 CORRECTED MACHINE-TOOL SETTINGS (CONVEX SIDE) *
****

BASIC TILT ANGLE :	CI =	0.3712125	radians
SWIVEL ANGLE :	CJ =	5.768892	radians
MACHINE ROOT ANGLE :	RGMA1M =	6.236861	radians
CRADLE ANGLE :	QC =	1.436096	radians
RADIAL SETTING :	SR =	113.6455	mm
SLIDING BASE :	DELTB =	23.87000	mm
MACHINE CENTER TO BACK:	DELTA =	3.767510	mm
BLANK OFFSET :	EM =	-39.63248	mm
CUTTING RATIO :	FM1 =	0.3020446	
CUTTER POINT RADIUS :	RCF =	114.9350	mm
CUTTER BLADE ANGLE :	PHIV1C =	-0.5410521	radians

****
* TABLE C.7 CORRECTIONS OF MACHINE-TOOL SETTINGS (CONVEX SIDE) *
****

BLANK OFFSET:	EM =	0.4875103	mm
MACHINE CENTER TO BACK:	DELTA =	0.5769074E-01	mm
SLIDING BASE :	DELTB =	0.0000000E+00	mm
MACHINE ROOT ANGLE :	RGMA1M =	0.3125239E-02	radians
RADIAL SETTING :	SR =	-0.3780939	mm
CRADLE ANGLE :	QC =	-0.8908187E-03	radians
SWIVEL ANGLE :	CJ =	0.2644968E-02	radians
TILT ANGLE :	CI =	-0.4977365E-02	radians

BIBLIOGRAPHY

1. Gleason Works: "G-Age T.M. User's Manual ", for the Gleason Automated Gear Evaluation System Used with Zeiss Coordinate Measuring Machines, Rochester, NY 1987.

2. Chambers R.O., and Brown R.E.," Coordinate Measurement of Bevel Gear Teeth", SAE Tchnical Paper Series 871645, International Off-Highway and Powerplant Congress, Milwaukee, Wisconsin, 1987.

3. Litvin, F. L.: "Theory of Gearing", NASA publications; RP-1212 (AVSCOM technical report; 88-c-035), 1989

4. Litvin, F.L., Y. Zhang, M. Lundy and C. Heine: "Determination of Settings of a Tilted Head Cutter for Generation of Hypoid and Spiral Bevel Gears", ASME J. of Mechanisms, Transmissions and Automation in Design Vol.1, Dec 1988, pp.495-500.

5. Litvin, F. L., Hong-Tao Lee: "Generation and Tooth Contact Analysis of Spiral Bevel Gears with Predesigned Parabolic Functions of Transmission Errors," NASA CR-4259 (AVSCOM TR-89-c-014), Nov., 1989

6. Litvin, F. L.,Y. Zhang,J. Kieffer,R. F. Handschuh, "Identification and Minimization of Deviations of Real Gear Tooth Surfaces", ASME Design Conference, 1989. Also accepted for publication in ASME J. of Mechanical Design.

7. Dongarra, J. J., J. R. Bunch, C. B. Moler, and G. W. Stewart, "LINPACK User's Guide", SIAM, Philadelphia, 1979.

8. Dudley, D.M.: "Gear Handbook: The Design, Manufacture, and Applications of Gears", McGRAW-HILL Book Company, Inc., New York, 1962.

9. Litvin, F. L.,C. Kuan, Y. Zhang, M. Lundy and W.-J Tsung: " Minimization of Deviations of Formate Hypoid Gears", J. of Surface Topography, in press, 1990.

10. Litvin, F. L., Y. Zhang, T. J. Krenzer and R. N. Goldrich: "Hypoid Gear Drive with Face - Milled Teeth: Conditions of Pinion Nonundercutting and Fillet Generation" ,AGMA Technical Paper, 1989 FTM 7.

NASA
National Aeronautics and Space Administration

Report Documentation Page

1. Report No.	2. Government Accession No.	3. Recipient's Catalog No.
NASA CR-4383 AVSCOM TR-91-C-021		

4. Title and Subtitle
Determination of Real Machine-Tool Settings and Minimization of Real Surface Deviation by Computerized Inspection

5. Report Date
July 1991

6. Performing Organization Code

7. Author(s)
Faydor L. Litvin, Chihping Kuan, and Yi Zhang

8. Performing Organization Report No.
None (E-6267)

10. Work Unit No.
1L162211A47A
505-63-36

9. Performing Organization Name and Address
University of Illinois at Chicago
Department of Mechanical Engineering
Chicago, Illinois 60616

11. Contract or Grant No.
NAG3-964

12. Sponsoring Agency Name and Address
Propulsion Directorate
U.S. Army Aviation Systems Command
Cleveland, Ohio 44135-3191
and
NASA Lewis Research Center
Cleveland, Ohio 44135-3191

13. Type of Report and Period Covered
Contractor Report
Final

14. Sponsoring Agency Code

15. Supplementary Notes
Project Manager, Robert F. Handschuh, Propulsion Directorate, U.S. Army Aviation Systems Command, NASA Lewis Research Center, (216) 433-3969.

16. Abstract

A numerical method is developed for the minimization of deviations of real tooth surfaces from the theoretical ones. The deviations are caused by errors of manufacturing, errors of installment of machine-tool settings and distortion of surfaces by heat-treatment. The deviations are determined by coordinate measurements of gear tooth surfaces. The minimization of deviations is based on the proper correction of initially applied machine-tool settings. The contents of accomplished research project cover the following topics:

(i) Description of the principle of coordinate measurements of gear tooth surfaces.
(ii) Derivation of theoretical tooth surfaces (with examples of surfaces of hypoid gears and references for spiral bevel gears).
(iii) Determination of the reference point and the grid.
(iv) Determination of deviations of real tooth surfaces at the points of the grid.
(v) Determination of required corrections of machine-tool settings for minimization of deviations.

The procedure for minimization of deviations is based on numerical solution of an overdetermined system of n linear equations in m unknowns ($m << n$), where n is the number of points of measurements and m is the number of parameters of applied machine-tool settings to be corrected. The developed approach is illustrated with numerical examples.

17. Key Words (Suggested by Author(s))	18. Distribution Statement
Gears Transmission Mechanical drives Gear teeth	Unclassified - Unlimited Subject Category 37

19. Security Classif. (of the report)	20. Security Classif. (of this page)	21. No. of pages	22. Price*
Unclassified	Unclassified	120	A06

*For sale by the National Technical Information Service, Springfield, Virginia 22161